

# Reaction between the Ionic Liquid BMP-TFSI and Li: Comparison between Monolayer Films and Thick Multilayer Films on Graphite (0001)

Katrin Forster-Tonigold, Florian Buchner, Axel Groß, and R. Jürgen Behm\*

Aiming at a molecular-scale understanding of the initial stages of the solid-electrolyte interphase (SEI) formation in Li-ion batteries, the chemical reaction of a monolayer of the ionic liquid 1-butyl-1-methylpyrrolidinium bis(trifluoromethylsulfonyl)imide (BMP-TFSI) adsorbed on a graphite (0001) substrate during postdeposition of Li and subsequent annealing has been investigated using a combined experimental and theoretical approach. For comparison, also the reaction between a bulk-like multilayer BMP-TFSI film and postdeposited Li is investigated. Employing X-Ray photoelectron spectroscopy and density functional theory-based calculations, it is found that postdeposition of Li at room temperature leads to a significant modification of both monolayer film

and bulk BMP-TFSI, including the formation of (adsorbed) molecular fragments, binary Li compounds, and desorption of volatile C- and F-containing species. The initial reaction with Li is highly exothermic and non- or little activated, and products are identified by comparison of experimental XP spectra and calculated core-level binding energies. Further reaction steps, leaving only binary Li compounds or comparable adsorbed species, are considerably activated and require annealing to >500–650 K, depending on the anion. Consequences of these results for the molecular-scale understanding of the initial stages of SEI formation in an electrochemical environment are discussed.

## 1. Introduction


The interaction of battery electrolytes with electrode surfaces is one of the key questions for the fundamental understanding of modern battery systems.<sup>[1–3]</sup> Among others, it is decisive for the stability of the electrolyte and for the formation, stability, and function of the solid–electrolyte interphase (SEI), which is indispensable as protective layer for the sustainable operation of modern battery systems.<sup>[4–12]</sup> Initially, information about the build-up of the SEI and its performance came mainly from purely electrochemical measurements.<sup>[4–6,8,9,13–15]</sup> While such measurements could provide detailed information on the performance of the SEI, insights about molecular aspects such as its molecular composition, the ongoing reactions, and the transport processes determining their performance remained elusive. In recent years, these topics have been increasingly studied by a wide variety of spectroscopic and microscopic techniques, both in postmortem

analysis (ex situ) and in situ or even operando conditions, that is, in the electrochemical environment or even under working conditions.<sup>[16–21]</sup> Furthermore, theoretical studies, including both density functional theory (DFT)-based calculations together with ab initio molecular dynamics (AIMD) simulations,<sup>[15,22–24]</sup> and also continuum modeling<sup>[25,26]</sup> provided increasing insights. The comparison between experimental and theoretical results often suffers, however, from the ill-defined structure and often also chemical composition of the electrode surface region in the experiments. In contrast, theoretical studies mostly deal with structurally well-defined, single-crystalline materials and model systems. Furthermore, also the theoretical description of the electrochemical environment is generally simplified. To lower these discrepancies, we had started a series of combined experimental and theoretical model studies. Aiming at a molecular/atomic level understanding of the processes at the electrode–electrolyte interface of Li-ion batteries, we had explored the chemical interaction between the battery-relevant ionic liquid (IL) 1-butyl-1-methylpyrrolidinium bis(trifluoromethylsulfonyl)imide (BMP-TFSI) as solvent, Li<sup>+</sup> as charge carrying shuttle ion, and structurally well defined, single-crystalline model electrodes of varying chemical activity such as Ag(111) or Au(111),<sup>[27–30]</sup> Cu(111),<sup>[30–32]</sup> graphite (0001),<sup>[30,33–36]</sup> and oxide surfaces such as TiO<sub>2</sub>(110)<sup>[37]</sup> or Co oxides.<sup>[38,39]</sup> Experimentally, this mainly involved a combination of scanning tunneling microscopy (STM) imaging and photoelectron spectroscopy (PES) measurements of the different adsorbate-covered surfaces resulting after vapor deposition of either Li and/or BMP-TFSI under different conditions and quantitative evaluation of the resulting surface structures and surface compositions. Theoretically, we determined energetically favorable decomposition products resulting from the interaction

K. Forster-Tonigold, F. Buchner, A. Groß, R. J. Behm  
Institute of Theoretical Chemistry  
Ulm University  
Oberberghof 7, D-89081 Ulm, Germany  
E-mail: juergen.behm@uni-ulm.de

K. Forster-Tonigold, F. Buchner, A. Groß  
Helmholtz Institute Ulm (HIU) Electrochemical Energy Storage  
Helmholtzstr. 11, D-89081 Ulm, Germany

K. Forster-Tonigold  
Karlsruhe Institute of Technology (KIT)  
P.O. Box 3640, D-76021 Karlsruhe, Germany

 © 2025 The Author(s). Batteries & Supercaps published by Wiley-VCH GmbH. This is an open access article under the terms of the Creative Commons Attribution License, which permits use, distribution and reproduction in any medium, provided the original work is properly cited.

between surface and deposits, in some cases also reaction barriers, their apparent structure in STM images, and most recently, also the binding energies of the core-level peaks resulting from possible reaction intermediates.<sup>[36,40]</sup> Finally, we also compared the composition of BMP-TFSI decomposition layers resulting from reaction with Li under vacuum conditions and upon electrochemical cycling in Li containing BMP-TFSI electrolyte in a combined electrochemical and surface science-type model study, using HOPG and a binder-free graphite powder material as substrate/electrode.<sup>[41]</sup>

In a recent combined experimental and theoretical study, we had determined the decomposition products resulting from the room temperature (RT) interaction of post-deposited Li and a thick BMP-TFSI film, where the Li is expected to directly interact with the BMP-TFSI without preceding adsorption on the underlying graphite (0001) substrate.<sup>[36]</sup> In that study, also the core-level binding energies had been determined for a large number of possible reaction products.<sup>[36]</sup> Experimentally, this involved a comprehensive X-ray photoelectron spectroscopy (XPS) characterization of the surface composition resulting after the reaction of the BMP-TFSI film and postdeposited Li<sup>0</sup>. Theoretically, this reaction was described as a reaction between a BMP-TFSI ion pair and one or more Li<sup>0</sup> atoms.<sup>[36]</sup> In the present work, we will extend this approach to the reaction between a BMP-TFSI monolayer film adsorbed on graphite (0001) and postdeposited Li, in a similar combined experimental and theoretical approach as described above. These two cases mainly differ by the fact that in the monolayer system, BMP, TFSI, and Li can all interact with the graphite substrate, while this is not possible for the multilayer system. This additional interaction may result in significant changes in the electronic structure of these species, which in turn may affect their reactivity. To assess the role and impact of kinetic barriers in the various reaction and desorption steps, we furthermore investigated the impact of thermal annealing steps to temperatures up to 700 K, both for the BMP-TFSI + Li monolayer system and the thick BMP-TFSI multilayer films. Theoretically, we identified the most stable reaction products resulting from the interaction of adsorbed BMP-TFSI and one or more coadsorbed Li atoms, which were relaxed in the unit cell before reaction, and their respective reaction energies. Subsequently, we calculated the core-level binding energies (BEs) for comparison with experimental XP spectra, using an approach that has been described in detail recently.<sup>[36,40]</sup> This allows a direct comparison between experimental XP spectra and characteristic binding energies of possible interaction or reaction products.

In the following, we will, after a brief description of the experimental and computational procedures in Section 4, first present and discuss XP spectra recorded on the graphite (0001) surface after deposition of a BMP-TFSI monolayer film at RT, after subsequent deposition of 0.7 and (in total) 1.4 monolayers (ML) of Li and after different annealing steps up to 650 K (Section 2.1.1). This is followed by comparable spectra recorded on a thick multilayer film of BMP-TFSI, including annealing steps up to 700 K (Section 2.1.2). Different from the monolayer case, this results in a direct interaction of Li<sup>0</sup> species with bulk BMP-TFSI, without preceding adsorption on the graphite (0001) substrate. Hence, a possible charge transfer is only possible to BMP-TFSI, in contrast

to the monolayer case, where charge can be transferred to the graphite (0001) substrate. It should be noted that the high temperature limits are close to the temperatures reported for thermal decomposition of neat BMP-TFSI or of 0.7 M solutions of Li-TFSI in BMP-TFSI of 650–700 K.<sup>[42,43]</sup> Subsequently, we present and discuss the results of calculations determining the structure and electronic properties of adsorbed Li, adsorbed BMP-TFSI, coadsorbed BMP-TFSI, and 1 or 3 Li atoms on graphite (0001), complemented by a similar calculation of a free-standing BMP-TFSI layer (Section 2.2.1). For these calculations, we used the unit cell that had been derived earlier for a saturated monolayer of BMP-TFSI on graphite (0001).<sup>[33]</sup> This includes also calculations of the changes in work function induced by the respective (co-)adsorbed species. In the next section (Section 2.2.2), we present calculations of different adlayer structures resulting from coadsorption of Li and BMP-TFSI and from the initial reaction between these species. In addition to the structures and reaction energies, this includes also calculated binding energies of characteristic core-level states of the different elements in these adsorbed species. These initial reactions can be considered as the first step in a chemical SEI formation. Finally, we show comparable results (stable structure, energy, and core-level BEs) for binary adsorbed species that correspond to the binary Li-containing species such as LiF, Li<sub>2</sub>O, or Li<sub>2</sub>S. In analogy to the above initial reaction products, these binary compounds can be considered as the last step in the reaction sequence describing chemical SEI formation. This section is followed by a brief discussion of the relevance of results obtained for such kind of idealized model systems and under idealized reaction conditions for the understanding of SEI formation on realistic systems, and of further improvements in the XPS analysis of complex surfaces such as the SEI layer (Section 2.3). Finally, we summarize the main findings of this study (Section 3).

## 2. Results

### 2.1. Thermally Activated Reaction between BMP-TFSI and Postdeposited Li

#### 2.1.1. Reaction Between a BMP-TFSI Monolayer Film and Postdeposited Li

In Figure 1, we present XP spectra of different core-level regions recorded upon vapor deposition of around 1 monolayer (ML) of BMP-TFSI on a graphite (0001) surface, subsequent deposition of Li, and finally stepwise annealing of the resulting adlayer up to 650 K. The spectra recorded upon BMP-TFSI vapor deposition, which are presented at the bottom of Figure 1, exhibit characteristic peaks, whose binding energies (BEs) are summarized in Table 1. Peaks in the C1s core-level region refer to the dominant C1s peak of the graphite substrate at 284.6 eV (gray), to carbon atoms with a nitrogen neighbor (C<sub>C-N</sub> peak at 286.9 eV, light red), which appears as a shoulder at the high BE side of the C<sub>graphite</sub> peak, and to the carbon atoms of the anion with fluorine neighbors (C<sub>TFSI</sub> at 292.9 eV, cyan). A third peak, which relates to the carbon atoms of the alkyl chain and of the pyrrolidinium ring

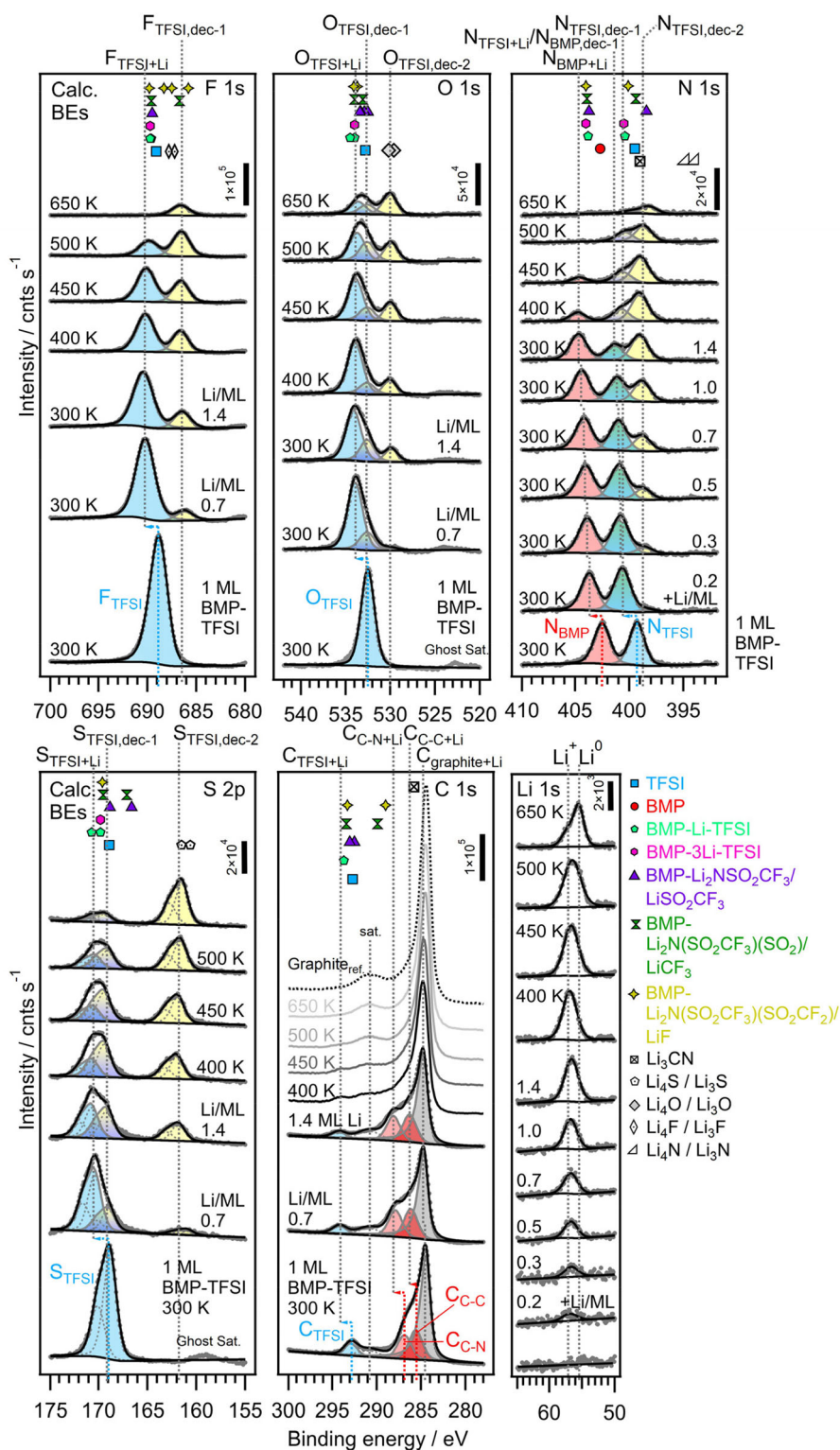


**Figure 1.** XPS spectra of the different core level regions (see figure) recorded (from bottom to top) after RT deposition of a monolayer film of BMP-TFSI on a graphite (0001) substrate, subsequent stepwise deposition of Li (see figure) and finally stepwise annealing to the temperatures indicated. Symbols at the top of the panels represent BEs calculated for adsorbed BMP-TFSI, for adsorbed initial reaction products (see Table 2) and for adsorbed binary Li compounds (see legend in the figure and Table 3).

of the cation with only carbon neighbors ( $C_{C-C}$  peak at about 285.6 eV, red) and which is hidden under the graphite substrate peak, is deduced by comparison with spectra recorded on the multilayer film in Figure 2. A satisfactory fit of the measured

spectra was achieved by setting the ratio of the BMP-TFSI-related  $C_{1s}$  components to 5:4:2, which is the nominal ratio of  $C_{C-C}/C_{C-N}/C_{TFSI}$  in BMP-TFSI.<sup>[27,44]</sup> In addition, a shake-up satellite of the main  $C_{graphite}$  peak appears at  $\approx 290.8$  eV.

**Table 1.** Binding energies of the core-level peaks measured on a monolayer BMP-TFSI covered graphite (0001) surface after deposition at RT or at 80 K and, for comparison, on a thick multilayer film of BMP-TFSI on graphite (0001) (Figure 2) and on a multilayer Mg film substrate (see also ref. [40]).

Denoted as	Monolayer film (RT) on graphite (0001) (this work)	Monolayer film (80 K) on graphite (0001) <sup>[34]</sup>	Monolayer film (RT) on graphite (0001) <sup>[33]</sup>	Thick multilayer film (RT) on graphite (0001) (this work)	Thick multilayer film (RT) on Mg/Ru (0001) <sup>[45]</sup>
C <sub>C-C</sub>	285.6	285.7	285.5	286.0	286.0
C <sub>C-N</sub>	286.9	286.7	286.7	287.3	287.3
C <sub>TFSI</sub>	292.9	292.8	292.8	293.5	293.5
C <sub>graphite</sub>	284.6/290.8	284.6/290.5	284.4/290.5	–	–
N <sub>BMP</sub>	402.5	402.7	402.7	403.3	403.3
N <sub>TFSI</sub>	399.3	399.5	399.5	400.0	400.0
F <sub>TFSI</sub>	688.9	688.9	–	689.6	689.6
S <sub>TFSI</sub>	168.8	168.9	168.9	169.6	169.6
O <sub>TFSI</sub>	532.5	532.6	–	533.3	533.3

The N1s spectrum of an as-deposited BMP-TFSI (sub)monolayer displays two contributions, where one is related to the nitrogen atom in the pyrrolidinium ring of the cation (N<sub>BMP</sub>, red) at 402.5 eV and the other one to that in the anion (N<sub>TFSI</sub>, cyan) at 399.3 eV, respectively (Figure 1). The N<sub>BMP</sub>/N<sub>TFSI</sub> intensity ratio of 1:1, together with the peaks in the C1s spectral range, verifies that BMP-TFSI is molecularly adsorbed on graphite (0001) at RT with a balanced cation to anion ratio. In addition, there are distinct peaks in the F1s, S2p, O1s core-level regions (F<sub>TFSI</sub>, S<sub>TFSI</sub>, O<sub>TFSI</sub>, filled cyan), which are characteristic for the CF<sub>3</sub> groups of the anion (F1s peak at 688.9 eV) and the SO<sub>2</sub> groups of the anion (S2p<sub>3/2</sub> peak at 168.8 eV, O1s peak at 532.5 eV).

The BEs are essentially identical to those of the core-level spectra recorded earlier upon deposition of a (sub-)monolayer BMP-TFSI film on pristine graphite (0001) at RT<sup>[33,35,45]</sup> or on a prelithiated HOPG substrate at 80 K (see Table 1).<sup>[34]</sup> The observation of identical spectra upon BMP-TFSI deposition on the pristine graphite (0001) at RT and on the prelithiated graphite (at 80 K) was basis of our previous claim that at 80 K surface segregation of Li dissolved in the bulk of HOPG is kinetically inhibited and that therefore BMP-TFSI adsorbs molecularly intact on the prelithiated graphite, without any measurable interaction with the (bulk dissolved) Li.<sup>[34]</sup>

Subsequent vapor deposition of about 0.7 monolayers (MLs) of Li on the BMP-TFSI covered surface at RT results in significant changes in the different regions, which are illustrated in the next higher spectra in Figure 1. For the F1s peak, we find an up-shift of the dominant peak to 690.2 eV, together with a severe loss in intensity. The dominant peak is attributed to a BMP-TFSI peak that due to its interaction with adsorbed Li is up-shifted in BE by about 1.4 eV (F<sub>TFSI,Li</sub>, cyan).<sup>[35]</sup> Reasons for this Li-induced shift will be discussed further in Section 2.2.2. Similar Li-induced up-shifts by about 1.3–1.7 eV are also observed for the TFSI-related N1s, O1s, S2p, and C1s peaks, and for the BMP-related N1s and C1s peaks. For the N1s peaks, the up-shift is most pronounced (1.7 eV), both for the TFSI-related and the BMP-related peak (the N1s spectra after Li deposition of 0.2, 0.3, and 0.5 ML, which are presented as well, reveal similar up-shifts). Also the main graphite peak at 284.6 eV reveals a small up-shift in BE by about 0.2–0.3 eV (C<sub>graphite+Li</sub>, indicated by the dashed lines) upon Li post-deposition, which back-shifts upon heating to >500 K. This was

assigned earlier to a rigid band shift due to charge transfer from Li to the top graphite layers<sup>[30,35]</sup> and will be discussed later in Section 2.2.1. At the same time, small peaks appear at 686.2, 530.1, 398.8, and 161.0 eV (filled yellow), which will be denoted as F<sub>dec-1</sub>, O<sub>dec-2</sub>, N<sub>dec-2</sub>, and S<sub>dec-2</sub>. These peaks had been assigned previously to inorganic products of Li-induced decomposition reactions such as LiF-, Li<sub>3</sub>N-, or Li<sub>2</sub>S- or Li<sub>2</sub>O-like species.<sup>[35]</sup> This will be discussed in more detail later (Section 2.2.2). For the O1s and S2p peaks, deconvolution reveals the formation of additional peaks at 532.6 eV (O<sub>dec-1</sub>, blue-yellow) and 169.0 eV (S<sub>dec-1</sub>, blue-yellow), respectively, which are most likely related to one or more molecular fragments resulting from the interaction with Li. Also, these assignments will be discussed in more detail in Section 2.2. Interestingly, the total intensity of the F1s peaks decreases significantly upon Li deposition, by slightly more than 20%, and the same occurs also for the C<sub>TFSI</sub> peak. Obviously, post-deposition of 0.7 ML Li at RT leads already to a significant formation of F- and C-containing volatile product species that can desorb instantaneously at RT. A similar trend (significant desorption) is observed for the intensity of the S-containing peaks. In contrast, for the O1s, N1s, and the BMP-related C1s peaks, the total intensities remain about constant. Obviously, in these latter cases, the intensity loss in the TFSI-related peaks is essentially compensated by an intensity gain in the new peaks, indicating that the decomposition of TFSI-like species results also in solid species that remain adsorbed on the surface. In addition, also volatile, S-containing molecules are formed that can desorb instantaneously.

Further deposition of Li (1.4 ML in total) enhances these trends, now with intensity losses for all core-level peaks. Again, the intensity loss is most pronounced for the F1s level (≈15% and less for the S2p levels (≈10%). But now also the intensities of the N1s, C1s, and O1s signals decrease by about 10% (N1s, C1s) and by about 5% (O1s), respectively. Obviously, at this point different volatile species are formed, which in combination lead to different total losses of the respective elements. Furthermore, also formation of solid decomposition products is enhanced, indicated by an increasing intensity of the different low-BE peaks, at the expense of the intensity in the BMP- or TFSI-related peaks. Obviously, the increased presence of Li adatoms favors the Li-induced decomposition of coadsorbed



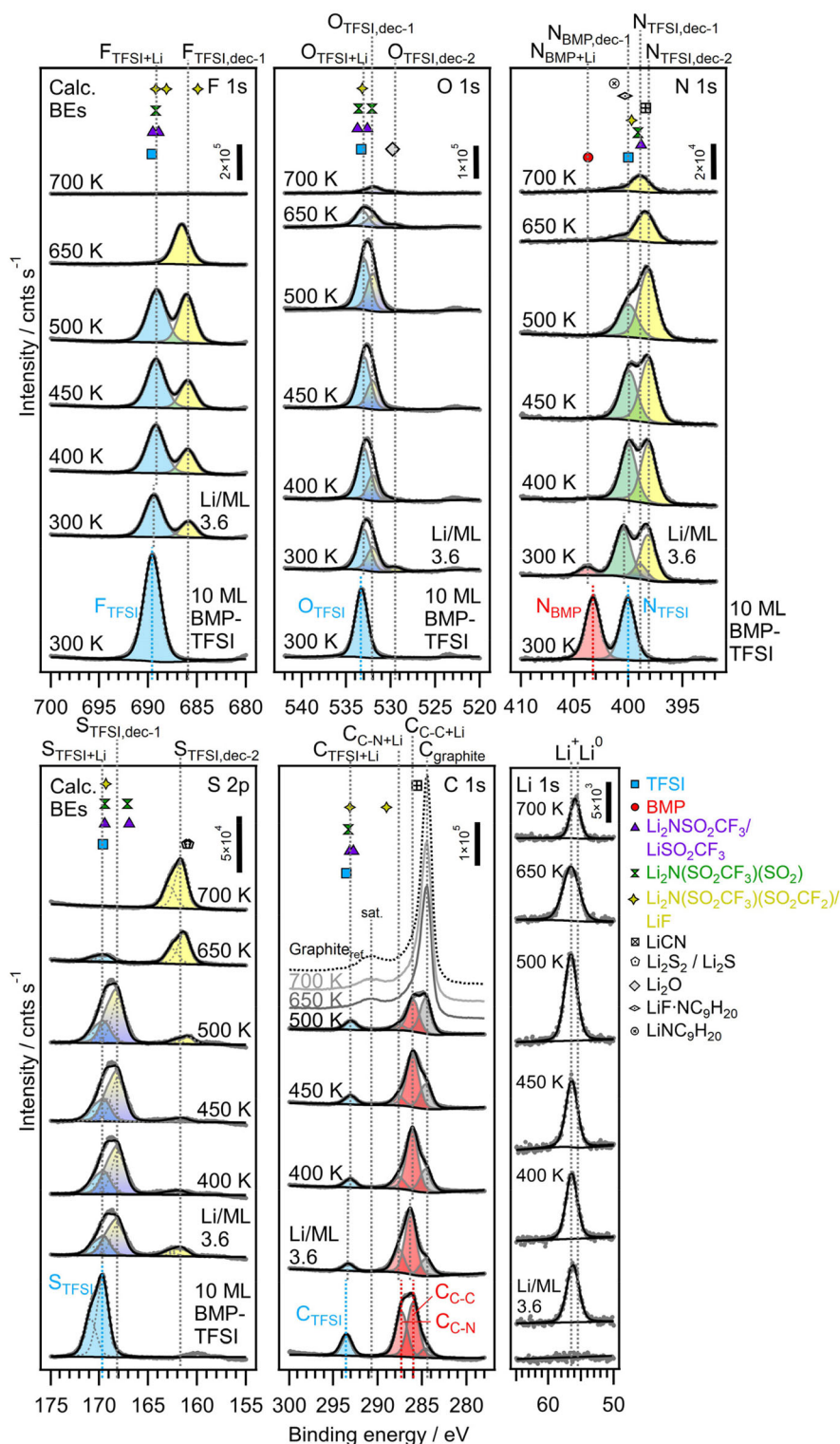


**Figure 2.** XP spectra of the different core level regions (see figure) recorded (from bottom to top) after RT deposition of a thick multilayer film of BMP-TFSI (10 ML) on a graphite (0001) substrate, subsequent deposition of Li (3.6 ML), and finally stepwise annealing to the temperatures indicated. Symbols at the top of the panels represent BEs calculated for adsorbed BMP-TFSI, for initial reaction products, and for binary Li compounds (see legend in the figure and ref. [36]).

BMP-TFSI, which is supported also by theoretical findings (see Section 2.2.2).

These trends continue upon annealing the adlayer-covered graphite (0001) sample to 400 K. Again we find losses in intensity, which are different for the different core levels. Most pronounced

losses are now observed for F ( $\approx -30\%$ ) and N ( $\approx -25\%$ ), while they are smaller for O ( $\approx -10\%$ ) and S ( $\approx -5\%$ ). The contributions from the IL to the C1s intensity can hardly be quantified anymore because of the increasing contribution from the main graphite peak and its satellite signal (see below). Obviously, the mix of

different molecular species desorbing during annealing has changed again as compared to desorption during Li deposition at RT, favoring now desorption of F- and N-containing species.

Similar to before, intensity losses occur mainly in the BMP-TFSI-related core-level peaks. Also these losses are not identical for the different core-level regions, which would be expected for desorption of molecular species. The BMP-related N1s peak decreases by about  $\frac{1}{3}$  during Li deposition, and annealing to 400 K leaves only slightly more than 20% of its initial intensity. In contrast, the TFSI-related N1s peak lost about 60% during Li deposition and disappeared almost completely upon annealing to 400 K. Obviously, reaction with Li affects adsorbed BMP in a different way than adsorbed TFSI. In addition, the new peak at lower BE ( $N_{\text{TFSI,dec-2}}$ , yellow), which started as a shoulder during Li deposition, turned into a distinct broad asymmetric peak upon annealing. Closer inspection reveals two components in this peak at about 400.7 and 399.0 eV, respectively. This decomposition behavior clearly differs from what would be expected from the trends in the F1s peak, where considerable amounts of TFSI-like species appeared still to be present even after 400 K annealing. These apparently contradictory findings were resolved recently for the interaction between Li and thick BMP-TFSI multilayer films<sup>[36]</sup> in a model, which is compatible also with the monolayer situation. According to that interpretation, interaction/reaction of Li with BMP leads to a product denoted as  $N_{\text{BMP,dec-1}}$ , which appears at only slightly higher BE than the  $N_{\text{TFSI+Li}}$  peak after RT deposition. This down-shift in BE is significantly more than a back-shift to the position of the  $N_{\text{BMP}}$  signal for the as-deposited IL. Therefore, it cannot simply result from the lack of interaction between adsorbed BMP and coadsorbed  $\text{Li}^{\delta+}$ , which could occur, for example, as a consequence of a reaction between adsorbed TFSI and  $\text{Li}^{\delta+}$ . During stepwise Li deposition of 0.2 up to 1.4 ML, this species coexists with the  $N_{\text{TFSI+Li}}$  peak (combined  $N_{\text{BMP,dec-1}}/N_{\text{TFSI+Li}}$  peak, filled green-cyan), which results in the slight broadening of that peak. After heating to 400 K, part of the TFSI is decomposed by reaction with Li, leading to the lower-BE peaks  $N_{\text{TFSI,dec-1}}$  (blue-yellow) and  $N_{\text{TFSI,dec-2}}$  (yellow) at 400.7 and 398.8 eV, respectively. At least part of the TFSI decomposition products exhibits molecular structures that closely resemble that of TFSI for most elements such as O, S, and in particular F, and thus differ only slightly from TFSI itself in these core-level spectra based on their BE. For  $N_{\text{TFSI+Li}}$ , in contrast, they clearly differ, as indicated by the new  $N_{\text{TFSI,dec-1}}$  peak, which emerges at 400 K. BMP appears to be somewhat more stable than TFSI, as the  $N_{\text{BMP+Li}}$  peak (red) does not disappear completely, although it loses much of its intensity upon annealing to 400 K. While we cannot exclude that the remaining BMP-related intensity is due to a molecular interaction/reaction product of BMP with rather similar chemical environment of the N atom as in BMP, we have no evidence for that. These aspects will be discussed in more detail in Section 2.2.2.

Upon further annealing cycles to 450, 500, and 650 K, the decomposition processes continue, resulting in a further loss of total intensity and in the intensity of the higher BE  $N_{\text{BMP+Li}}$  (red) and  $N_{\text{TFSI+Li}}/N_{\text{BMP,dec-1}}$  (cyan-green) peaks. Here, it should be kept in mind that the evaporation temperature of neat BMP-TFSI during deposition was 450 K, which resulted in

deposition rates of about  $0.1 \text{ ML min}^{-1}$ , and temperatures between 450 and 500 K were reported also for second layer desorption of BMP-TFSI from HOPG.<sup>[30]</sup> Therefore, at temperatures  $\geq 450 \text{ K}$ , adsorbed BMP-TFSI can exist only if stabilized by interactions with the graphite surface or, more likely, with coadsorbed Li. The molecular species represented by the  $N_{\text{BMP+Li}}$  (red) and  $N_{\text{TFSI+Li}}/N_{\text{BMP,dec-1}}$  (cyan-green) peaks largely disappeared upon annealing to 450 K and were completely absent after annealing to 500 K, forming either volatile compounds or decomposing into smaller solid fragments and finally into the compounds represented by the  $N_{\text{TFSI,dec-1}}$  (blue-yellow) and  $N_{\text{TFSI,dec-2}}$  (yellow) peaks. Here, we assign the  $N_{\text{TFSI,dec-2}}$  peak to one or more rather stable binary compounds, most likely LiCN (see discussion in Section 2.2.2). Annealing to 650 K finally leads to the disappearance of the  $N_{\text{TFSI,dec-1}}$  peak, and also much of the  $N_{\text{TFSI,dec-2}}$  peak desorbed.

For the F1s region, we find a significant loss in intensity of the  $F_{\text{TFSI+Li}}$  peak (cyan) upon annealing to 500 K, and it completely disappeared upon annealing to 650 K. In this latter annealing step, also the low BE  $F_{\text{TFSI,dec-1}}$  peak, which in previous steps had grown due to the decomposition of the molecular species represented by the  $F_{\text{TFSI+Li}}$  peak, lost much of its intensity. Apparently, the underlying binary compound, most likely adsorbed LiF-like species, started to (reactively) desorb under these conditions.

In the O1s region, in contrast, the TFSI-related  $O_{\text{TFSI+Li}}$  peak (cyan) remained about stable upon annealing to 400 K, and also annealing to higher temperatures up to 500 K did not cause dramatic changes. Only upon annealing to 650 K, it lost a significant amount of its intensity. Considering the very different trends in the N1s and F1s peaks, the  $O_{\text{TFSI+Li}}$  peak must contain contributions from rather stable adsorbed species, which are different from coadsorbed TFSI and Li, but where the local environment of the O atoms closely resembles that in TFSI. The lower-BE  $O_{\text{TFSI,dec-1}}$  (blue-yellow) and  $O_{\text{TFSI,dec-2}}$  (yellow) peaks even grew in intensity up to 650 K annealing, indicating that they result from decomposition of the TFSI-like species, and that the increase in these fragments due to decomposition of TFSI-like species can even overcompensate possible losses due to desorption. Only upon annealing to 650 K, the  $O_{\text{TFSI,dec-1}}$  peak loses in intensity, while the  $O_{\text{TFSI,dec-2}}$  peak continues to grow. Hence, the adsorbed  $\text{Li}_2\text{O}$ -like species reflected by the latter peak (see above) appears to be stable up to 650 K.

For the S2p region, the high-BE  $S_{\text{TFSI+Li}}$  peak (cyan), which is related to adsorbed TFSI-like species, loses some intensity upon annealing to 400 K, but much less than, for example, the  $N_{\text{TFSI+Li}}$  peak. Obviously, similar to the  $O_{\text{TFSI+Li}}$  (blue-yellow) peak, this signal contains contributions from adsorbed molecular fragments with a rather similar local environment of the S atoms as in TFSI, which appear at essentially the same BE, but is more stable than coadsorbed, interacting TFSI and Li. Another fragment, represented by the  $S_{\text{TFSI,dec-1}}$  peak, changes little upon annealing to 400 K. Correspondingly, also the decomposition product represented by the  $S_{\text{TFSI,dec-2}}$  peak, increases little in coverage. Further annealing to 450 and 500 K results in a slight loss of intensity in the molecular species represented by the  $S_{\text{TFSI+Li}}$  (cyan) and  $S_{\text{TFSI,dec-1}}$  (blue-yellow) peaks, with a corresponding growth of the

$S_{\text{TFSI,dec-2}}$  peak. Even after annealing to 650 K, however, the higher-BE peaks have not completely disappeared, while the low BE- $S_{\text{TFSI,dec-2}}$  peak increased further, though this could not fully compensate for the intensity loss in the higher-BE peaks. Hence, thermal decomposition of the molecular fragments in the  $S_{\text{TFSI,dec-1}}$  peak results partly in stable binary compound species, most likely adsorbed  $\text{Li}_2\text{S}$ -like species, while another part leads to volatile species that desorb during annealing.

For the C1s peaks, annealing to 400 K leads to a significant loss of intensity in the  $C_{\text{TFSI}}$  peak (cyan), and upon annealing to 450 K, this peak has completely disappeared. Hence, at this point, TFSI-like species, in particular the  $\text{CF}_3$  groups, are fully decomposed. This result is not only consistent with our findings for the other elements, in particular for the F1s signal, which indicated already decomposition of TFSI-like species and molecular fragments under these conditions, but goes beyond them as it shows that also  $\text{CF}_3$  groups have disappeared. For the other BMP-TFSI-related peaks, a quantitative evaluation was hardly possible because of the dominant contribution from the graphite substrate peak (284.6 eV) and the related satellite at 290.5 eV, which increase upon increasing desorption of BMP-TFSI decomposition products. Qualitatively, the spectra indicate that most of the carbon-containing BMP-TFSI decomposition products have disappeared after 450 K annealing, which would be consistent with the observation of more stable binary Li compounds in the other core-level regions under these conditions.

Finally, the Li1s peak, which is located at 56.7 eV upon Li deposition, remains about constant in BE upon annealing to 400 and 450 K, while the intensity appears to increase slightly. Most simply, this increase in intensity is due to the desorption of volatile F- and N-containing species discussed above. The considerable intensity increase upon annealing to 500 K is at least partly due to the generally higher intensity in this measurement (see above). In addition, the peak seems to broaden to lower BEs. Annealing to 650 K, finally, leads to the formation of an asymmetric peak shape with its maximum at lower BE, at 55.5 eV, together with a significant intensity loss. This peak, which would be compatible with a metallic  $\text{Li}^0$  component,<sup>[46]</sup> seems to form already during annealing to 500 K, where it leads to the peak broadening. Both the peak shift and the loss in intensity can be explained by decomposition of Li-containing compounds, leaving  $\text{Li}^0$  species in the surface region and below. The loss of Li intensity is then due to  $\text{Li}^0$  dissolution into deeper regions, where it is less or no more visible by XPS.

In total, postdeposition of Li on a monolayer BMP-TFSI-covered graphite (0001) surface at RT leads to an up-shift in BE of the BMP-TFSI-related core-level signals by about 1.3–1.7 eV, caused by the interaction with the coadsorbed  $\text{Li}^{\delta+}$ . Furthermore, it results in partial reaction of coadsorbed BMP-TFSI and Li, leading to modifications in the BMP-TFSI related peaks, to the formation of new peaks at lower BE ( $F_{\text{dec-1}}$ ,  $O_{\text{dec-2}}$ ,  $N_{\text{dec-2}}$ ,  $S_{\text{dec-2}}$ , yellow), and to a loss in total F1s and C1s intensity due to the desorption of volatile F- and C-containing species. The resulting molecular fragments exhibit BEs that for some elements are very similar to those of the coadsorbed BMP-TFSI and Li species. For the O1s, S2p, and most clearly for the N1s peak, they can

be clearly distinguished, indicating that the initial reaction affects mainly the local environment of these atoms, mainly of the adsorbed TFSI species, but possibly also of the adsorbed BMP species. Thermal activation of the resulting adlayer by annealing to 400 K results in almost complete conversion of the adsorbed BMP-TFSI-like species into molecular fragments and into the binary compound species. Further annealing to 450 and 500 K causes stepwise decomposition of these molecular reaction intermediates into the binary Li compounds or closely related species. Upon annealing to 650 K, also LiF- and LiCN-like adsorbed species desorb completely, while O- and S-containing compounds are still present on the surface. Further aspects of the decomposition processes are discussed in Section 2.2.2.

### 2.1.2. Reaction between a BMP-TFSI Multilayer Film and Postdeposited Li

Spectra recorded upon RT deposition of a thick multilayer film (10 ML) of BMP-TFSI, followed by postdeposition of Li (3.6 ML) at RT and finally stepwise annealing of that surface up to 700 K, are presented in Figure 2. Since spectra recorded upon RT deposition of BMP-TFSI and increasing postdeposition of Li, up to 3.6 ML, were already presented and discussed previously,<sup>[36]</sup> the trends during these phases will only be summarized in the following. After RT deposition of BMP-TFSI, the spectra closely resemble those obtained from a monolayer film-covered sample, except for a slight up-shift to higher BEs by about 0.6–0.7 eV and the absence of the pronounced peak in the C1s region at 284.6 eV related to the graphite (0001) substrate (see Section 2.1.1). The BEs (see Table 1) and the intensity ratios of the different peaks underline that also for thicker films BMP-TFSI adsorbs molecularly intact at RT. The up-shift in BE relative to the monolayer peaks can be attributed to a vacuum level pinning effect,<sup>[36,40,47]</sup> where the core-level states of the weakly binding adsorbate are coupled to the vacuum level rather than to the Fermi level of the substrate.<sup>[48,49]</sup>

Upon Li postdeposition (3.6 ML) and subsequent annealing, the BMP-TFSI-related peaks stepwise decay in intensity and additional peaks emerge at lower BEs. Different from reaction with the adsorbed monolayer, there is no general Li-induced shift of the peaks related to the BMP-TFSI bulk. Only for the higher-BE  $N_{\text{BMP}}$  peak, we find a small up-shift (see below). The absence of a general shift can be rationalized by the absence of the surface dipole generated by the charge transfer from adsorbed  $\text{Li}^{\delta+}$  to the top-most graphite (0001) layer. Accordingly, the shift of the  $N_{\text{BMP+Li}}$  peak (red) must be due to a direct chemical interaction between Li and BMP.

In the N1s region, deposition of 3.6 ML Li leads to a slight up-shift in BE of the BMP-related peak at 403.3 eV by about 0.5 eV. It also loses most of its intensity, indicating almost complete decomposition of the BMP cations. This seems to be different from the monolayer situation (Figure 1), where Li postdeposition caused a much smaller loss of BMP-related N1s intensity. This difference may, however, be related to the lower amount of Li postdeposition on the monolayer film as compared to the multilayer film. The TFSI-related signal at 400.0 eV also seems to shift to

slightly higher BE (400.5 eV) upon Li deposition and loses intensity, although much less than the BMP-related signal. As discussed already in Section 2.1.1, we had shown recently in a series of stepwise increasing Li doses that an interaction/reaction product between BMP and Li appears at this position ( $N_{\text{BMP,dec-1}}$ , green), which upon increasing Li deposition stepwise replaces the original TFSI-related peak.<sup>[36]</sup> In fact,  $\text{Li-NC}_9\text{H}_{20}$  and  $\text{LiF-NC}_9\text{H}_{20}$  species, where Li or LiF interact with BMP, were found to exhibit BEs exactly in this range.<sup>[36]</sup> After 3.6 ML Li deposition, this process is almost completed. Furthermore, two new peaks appear at 398.2 and 398.9 eV, which were assigned to species resulting from the reaction between Li and TFSI (398.9 eV:  $N_{\text{TFSI,dec-1}}$  (blue-yellow) and 398.2 eV:  $N_{\text{TFSI,dec-2}}$ , yellow).<sup>[36]</sup> This assignment was supported also by the intensity balance of the BMP-related peaks and the TFSI-related peaks during stepwise increasing Li deposition, which showed a constant total intensity for each of these species.<sup>[36]</sup> Hence, losses due to desorption of N-containing species and thus the formation of volatile N-containing reaction products during Li deposition must be small.

Upon annealing to 400 K, the BMP-related  $N_{\text{BMP+Li}}$  peak (red) is no longer detected. Hence, at this point, the molecular BMP-like species were fully converted to the  $\text{BMP}_{\text{dec-1}}$  species, and accordingly, the peak at 400.5 eV increased slightly in intensity. Also one of the TFSI decomposition products ( $\text{TFSI}_{\text{dec-1}}$ , blue-yellow) disappeared. Nevertheless, the total N1s intensity remained about constant, indicating that the formation of volatile reaction products is still small at this point. This is different from the monolayer case, where the loss in N1s intensity due to desorption was considerable after similar treatment. Upon annealing to 450 K, there appears to be a slight intensity transfer from the higher BE component ( $N_{\text{BMP,dec-1}}$ , green) to the lower BE component ( $N_{\text{TFSI,dec-2}}$ , yellow), while the total intensity remains about constant. Hence, upon annealing to 450 K, the lower BE component, which was related above to a TFSI decomposition product, may contain also contributions from a BMP decomposition product, which resulted from the reaction between the  $\text{BMP}_{\text{dec-1}}$  species (green) and Li. Upon annealing to 500 K, these processes continue and become more pronounced. But still, there are no significant changes in the total N1s intensity. Hence, so far there was no desorption of N-containing species. Here, we should note that all spectra recorded after 500 K annealing of the multilayer film show a higher intensity than before and after that measurement, indicating that this is due to a systematic effect of the measurement.

Annealing to 650 K results in the complete disappearance of the  $N_{\text{BMP,dec-1}}$ -related peak (green) and hence full decomposition of this species. Also, the low BE component ( $N_{\text{TFSI,dec-2}}$ , yellow), which as stated above may also contain now some BMP decomposition products, loses significantly in intensity due to the desorption of reaction products. Obviously, both BMP- and TFSI-related reaction products have further reacted into species that are volatile at these temperatures. The considerable desorption of BMP-TFSI-related species is indicated also by the appearance of the graphite-related C1s peak at 284.6 eV. Hence, at this point, the system starts to resemble the monolayer system rather than bulk BMP-TFSI. Finally, upon annealing to 700 K, the low-BE peak has decayed further in intensity, indicative of ongoing

desorption of volatile reaction products of the TFSI- and BMP-related reaction products. It also shifts to slightly higher BE, which may either be due to direct interaction with the graphite substrate, or caused by dominant desorption of TFSI reaction products ( $N_{\text{TFSI-2}}$ , yellow), leaving only decomposition products of the  $\text{BMP}_{\text{dec-1}}$  species on the surface, or vice versa. From the small shift in BE alone, however, we cannot distinguish between these possibilities.

In total, the N1s spectra in Figure 2 revealed a complex reaction scheme for the Li-induced decomposition of bulk BMP-TFSI. In the presence of sufficient Li, both BMP and TFSI can largely react into solid, mostly molecular reaction products already at RT. This process continues upon thermal activation. Significant formation of volatile N-containing reaction products is observed only upon annealing to 650 K and higher temperatures. The trends for Li-induced decomposition largely follow the trends obtained and discussed before for the reaction between an adsorbed BMP-TFSI monolayer and Li (Figure 1). There are, however, also some differences in the reaction behavior, both in the RT reaction behavior and upon annealing. Most prominent, the BMP-related peak at higher BE (403.3 eV) disappeared only upon annealing to 450–500 K for the monolayer reaction, while for the multilayer situation, this peak disappeared largely already during Li post-deposition at RT.

In the F1s region, Li deposition leads to an additional peak at about 685.9 eV ( $F_{\text{TFSI,dec-1}}$ , yellow), while except for a considerable intensity loss there is no significant change in the TFSI-related peak at 689.4 eV ( $F_{\text{TFSI+Li}}$ , cyan). Based on its BE, the new peak could be due to the formation of LiF, whose BE was reported to be in the range of  $685.0 \pm 0.2$  eV.<sup>[46]</sup> Considering that at RT desorption of BMP-TFSI is negligible, the total loss in F1s intensity of about 40% upon Li deposition was attributed to the formation and desorption of F-containing, but N-free (see above) reaction products such as  $\text{C}_2\text{F}_4$ , which are volatile already at RT.<sup>[36]</sup> Nevertheless, most of the remaining F1s intensity is in the TFSI-related peak, indicating that under these conditions the formation of adsorbed stable reaction products is still slow. Stepwise annealing up to 450 K results in little change. Only upon annealing to 500 K, we find some intensity transfer from the high-BE  $F_{\text{TFSI+Li}}$  peak (cyan) to the low-BE  $F_{\text{TFSI,dec-1}}$  peak (yellow), indicating that at this temperature another reaction pathway opens up. Annealing to 650 K leads to the complete disappearance of the  $F_{\text{TFSI+Li}}$  peak, together with a much smaller intensity loss ( $\approx 10\%$ ) in the low-BE  $F_{\text{TFSI,dec-1}}$  peak. We cannot decide from these data, however, whether the desorption of the TFSI-related species occurs directly or whether part of them converts into the  $F_{\text{TFSI,dec-1}}$  species, together with desorption of the  $F_{\text{TFSI,dec-1}}$  related species. Together with these intensity losses, the  $F_{\text{TFSI,dec-1}}$  peak shifts also to slightly higher BE, which can result either from a modification of the species underlying the  $F_{\text{TFSI,dec-1}}$  peak or from decomposition of species in the previous  $F_{\text{TFSI+Li}}$  peak. Finally, upon annealing to 700 K, also this latter peak disappears completely. The identity of possible reaction product species resulting in the two F1s peaks will be discussed in more detail in Section 2.2.2.

Comparison with the F1s data obtained for the reaction between an adsorbed BMP-TFSI monolayer and Li in Figure 1



reveals little difference in the reaction behavior, despite the different BMP-TFSI:Li ratio. At least for the reaction pathways leading to F-containing reaction intermediates/products, the direct interaction with the graphite substrate does not seem to cause major changes in the reaction behavior between Li and BMP-TFSI. This is important also from fundamental aspects, since for the monolayer situation the reaction starts from coadsorbed and therefore positively charged Li,<sup>[35]</sup> while for the thick multilayer film Li arrives as a neutral atomic species. Hence, there is a difference in the initial state of Li in the two cases, which, however, seems to have little impact on the reaction behavior.

The spectrum in the O1s region shows a broadening of the TFSI-related peak at about 533.3 eV ( $O_{\text{TFSI+Li}}$ ) upon Li deposition and a weak peak at about 529.6 eV ( $O_{\text{TFSI,dec-2r}}$ , yellow). Deconvolution of the main peak, which is centered at around 532.5 eV, resolves two components, one at 533.0 eV ( $O_{\text{TFSI+Li}}$ , cyan) and one at 532.0 eV ( $O_{\text{TFSI,dec-1r}}$ , blue-yellow). The  $O_{\text{TFSI,dec-1}}$  component is likely related to a molecular decomposition product of TFSI, while the peak at around 530 eV is most likely due to an adsorbed inorganic compound such as  $\text{Li}_2\text{O}$ .<sup>[36]</sup> The total intensity of the O1s peaks remains constant. Hence, there is no desorption of O-containing species during Li postdeposition at RT. Upon annealing to 400 K, there are no significant changes, except for the disappearance of the low-BE peak. Also, further annealing to 450 and 500 K has no significant effect on the composition of the high-BE peak, and the low-BE peak remains absent. Only upon annealing to 650 K, we find a significant loss of total O1s intensity by about 60%. The intensity ratio in the two components remains, however, about constant. Finally, upon annealing to 700 K, most of the O1s intensity is lost. The slight down-shift in BE seems to indicate that the remaining intensity is solely due to the lower-BE component (blue-yellow) in the combined  $O_{\text{TFSI+Li}}/O_{\text{TFSI,dec-1}}$  peak. The comparable trend in the relative loss of intensity in the N1s and O1s peaks is most simply explained by the desorption of both N- and O-containing species.

Comparison with the monolayer spectra in Figure 1 shows that the low BE peak at about 530.0 eV is much more pronounced in the monolayer system, indicating that  $\text{Li}_2\text{O}$  formation is more facile in that case. This peak, which due to the Li-induced up-shift of the TFSI-related peaks in the monolayer system is also better separated in the monolayer spectra, disappears at higher annealing temperatures, while in the monolayer spectra it remains up to 650 K annealing, the highest temperature in those measurements. Furthermore, also the intensity ratio of the two components in the higher-BE peak ( $O_{\text{TFSI+Li}}$  (cyan),  $O_{\text{TFSI,dec-1}}$  (blue-yellow)) seems to be different in the multilayer than in the monolayer spectra upon annealing, with a lower relative intensity in the  $O_{\text{TFSI+Li}}$  component (cyan) than in the  $O_{\text{TFSI,dec-1}}$  component (blue-yellow). On the other hand, similar to the monolayer spectra in Figure 1, the intensity loss in the higher-BE peak ( $O_{\text{TFSI+Li}}$  and  $O_{\text{TFSI,dec-1}}$ ) occurs mostly upon 650 K annealing. Hence, the direct interaction with the graphite substrate does not seem to stabilize the fragments against (reactive) desorption.

In the S2p region, Li deposition leads to an additional peak at about 161.6 eV ( $S_{\text{TFSI,dec-2r}}$ , yellow), which had previously been assigned to  $\text{Li}_2\text{S}$ -like species.<sup>[36]</sup> This assignment will be discussed in more detail in Section 2.2.2. Furthermore, the broadening of

the TFSI-related peak to lower BEs points to the formation of another component with slightly lower BE. Deconvolution results in a peak centered at 168.0 eV ( $S_{\text{TFSI,dec-1r}}$ , blue-yellow), in addition to the TFSI-related  $S_{\text{TFSI+Li}}$  peak at 169.5 eV. Upon annealing to 400, 450, and 500 K, we find little change in the total S2p intensity, resembling the behavior of the N1s core levels. Also, the different components do not change significantly, neither in intensity nor in BE. Only upon annealing to 650 K we find a drastic decrease of the high-BE peaks ( $S_{\text{TFSI+Li}}$  and  $S_{\text{TFSI,dec-1r}}$ ), accompanied by a significant increase of the low-BE  $S_{\text{TFSI,dec-2}}$  peak. Obviously, under these conditions, a large fraction of the molecular species in the high-BE peaks reacts to the species responsible for the low-BE peak. Furthermore, based on the significant loss in total intensity, also desorption of species volatile under these conditions takes place as a competing process. Annealing to 700 K finally results in the complete disappearance of the high-BE peak, while the low-BE peak seems to be stable. The apparent increase in intensity of the  $S_{\text{TFSI,dec-1}}$  peak (yellow) at this point may be due to the desorption of S-free covering species, as its intensity increase is more than the transfer from the former high-BE peak could account for.

There is some difference in the S2p data obtained for the reaction between an adsorbed BMP-TFSI monolayer and Li in Figure 1. The relative intensity in the low-BE peak ( $S_{\text{TFSI,dec-2r}}$ , yellow) upon Li post-deposition and upon annealing up to 500 K, relative to that in the high-BE peak, is significantly higher in the monolayer than in the multilayer measurements. Most simply, this difference with respect to our findings for the other core levels may be explained by the formation of molecular, S-containing reaction intermediates with a local environment of the S atoms that is  $\text{Li}_2\text{S}$ -like. This will lead to an S2p signal in the range of the  $S_{\text{TFSI,dec-2}}$  signal, while the signals of the related N and O atoms still appear in the  $O_{\text{TFSI,dec-1}}$  and  $N_{\text{TFSI,dec-1}}$  ranges. This difference between the monolayer and multilayer experiments may be due to the direct interaction with the graphite substrate in the monolayer spectra, but may alternatively also result from the different BMP-TFSI:Li ratios. Hence, for the S2p core level, it is less obvious whether the presence of graphite results in a modification of the reaction behavior between BMP-TFSI and Li.

Changes in the C1s spectra upon Li postdeposition and annealing can be summarized as follows: Deposition of 3.6 ML Li induces already a significant intensity loss in the  $C_{\text{TFSI}}$  (cyan) peak, while during subsequent annealing up to 500 K this peak at around 293 eV ( $C_{\text{TFSI+Li}}$ , cyan) is about stable, both in intensity and in BE. It disappears only upon annealing to 650 K. The  $C_{\text{C-C}}$  (red) peak at about 286 eV is largely stable up to 450 K; it loses much of its intensity upon annealing to 500 K. Also, these species are no longer detectable upon annealing to 650 K. At this point, evaluation of the  $C_{\text{C-C}}$  peak is hindered also by the strongly increasing graphite-related signal (284.6 eV, gray), due to desorption of much of the multilayer and its decomposition products. The same trend is observed also for the  $C_{\text{C-N}}$  peak at 287.6 eV (light red). Hence, after annealing most of the C-containing decomposition products of BMP-TFSI and Li have desorbed. Remaining quantities are below the detection limit given by the broad signal of graphite and the related satellite (290.8 eV).

Finally, the Li1s spectra do not show any peak shifts or broadening up to 500 K annealing. Hence, up to that point, the electronic state of the Li species, which based on its BE of 56.4 eV is strongly positively charged ( $\text{Li}^+$ ), is stable. Annealing to 650 K leads to a broadening of the Li1s peak at the lower-BE side. After annealing to 700 K, which goes along with a significant intensity loss, only a narrow peak with its maximum at about 55.9 eV remains. This behavior, which closely resembles that in the Li1s monolayer spectra, can be explained in a similar way, namely by (reactive) desorption of most of the Li-containing BMP-TFSI decomposition products upon annealing to 650 and 700 K, leaving mostly adsorbed or dissolved  $\text{Li}^0$  species on the graphite surface.

In total, reaction between the multilayer BMP-TFSI film on graphite (0001) and Li during post-deposition of Li (3.6 ML) at RT results already in the significant decomposition of adsorbed  $\text{BMP} + \text{Li}$  and  $\text{TFSI} + \text{Li}$  species into volatile C- and F-containing species, into molecular fragments and to some extent also already into more stable binary compound species. The molecular fragments exhibit BEs, which for most of their elements are either identical or rather close ( $\text{O}_{\text{TFSI,dec-1}}$ ,  $\text{S}_{\text{TFSI,dec-1}}$ , blue-yellow) in BE and hence in local environment to the coadsorbed BMP-TFSI and Li ( $\text{F}_{\text{TFSI+Li}}$ ,  $\text{O}_{\text{TFSI+Li}}$ ,  $\text{S}_{\text{TFSI+Li}}$ ,  $\text{C}_{\text{TFSI+Li}}$ , cyan) species. Only in the BMP-related N1s peak they can be clearly distinguished ( $\text{N}_{\text{BMP}}$ , red,  $\text{N}_{\text{BMP,dec-1}}$ , green), indicating that this initial decomposition affects mainly the local environment of the N atoms in the adsorbed BMP species. In this respect, there is little difference to the decomposition behavior of BMP observed for the monolayer film, except that in the monolayer case this

requires annealing, while for reaction with bulk BMP-TFSI this occurs largely already during Li postdeposition at RT. Further annealing to 450 and 500 K causes stepwise decomposition of these molecular reaction intermediates into binary Li compounds or closely related species. Upon annealing to 650 K, also  $\text{LiF}$ - and  $\text{LiCN}$ -like adsorbed species (reactively) desorb completely, while O- and S-containing compounds are still present on the surface. Also these trends are very close to the decomposition behavior observed for the monolayer film, indicating that the interaction of the adsorbed species with the graphite (0001) surface has little effect on their decomposition behavior. Also, there seems to be little difference in the interaction with an impinging  $\text{Li}^0$  species, as encountered for the multilayer film, or with a coadsorbed  $\text{Li}^{\delta+}$  in the case of the monolayer film. Hence, the different initial states in these two cases seem to have little effect on the reactive decomposition behavior of BMP-TFSI, and the same is true also for the interaction of BMP-TFSI and its reaction products with the graphite (0001) substrate.

## 2.2. Calculated Electronic Structure and Binding Energies

### 2.2.1. Electronic Structure of a BMP-TFSI Monolayer and Li on Graphite

With respect to the calculations, we are mainly interested in the changes in the electronic properties induced by adsorption of BMP-TFSI and its coadsorption with Li, both of surface properties and of characteristic properties of BMP-TFSI. **Figure 3** summarizes

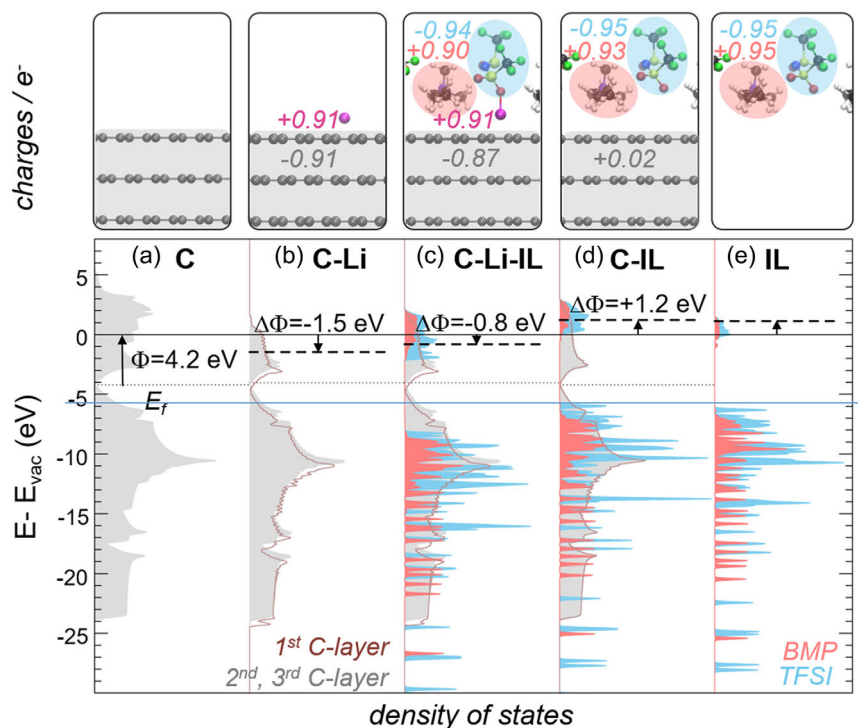


**Figure 3.** Bader charges and density of states projected on the atoms of BMP (red), TFSI (blue), and graphite (gray) for a) graphite (0001), b) Li adsorbed on graphite (0001), c) Li trapped between graphite (0001) and IL, d) IL adsorbed on graphite (0001), and e) a free-standing 2D IL layer. The dotted line denotes the Fermi energy ( $E_F$ ). All energies are referred to the vacuum level of the bare graphite surface. The respective vacuum levels of the various adsorption structures are shown as dashed lines.

the electronic properties of different adsorption complexes on graphite (0001) in the monolayer film (see “Computation” under Experimental Section), including the Bader charges, the densities of states of the different adsorption complexes, and their respective work function changes. In addition to the properties of the bare basal plane of graphite (a), Figure 3 shows these features for Li (b) or BMP-TFSI (d) or both (c) adsorbed on the graphite (0001) surface. For comparison, it also shows the densities of states for a free-standing 2D IL layer (e) fixed in the geometry it adopts in the adsorption complex.

As expected, adsorption of Li (Figure 3b) leads to a charge transfer from the alkali metal atom to the topmost graphite layer, which results in a decrease of the work function and a rigid band shift of the valence band with respect to the Fermi energy ( $E_f$ ), specifically of the topmost graphite layer.

Adsorption of BMP-TFSI in the monolayer structure causes hardly any changes in the density of states projected onto the atoms of BMP, TFSI, and graphite (Figure 3a,d,e), reflecting non-covalent interactions between BMP-TFSI and the graphite surface.<sup>[33]</sup> As the anions adsorb at a larger distance from the surface than the cations in this monolayer, adsorbed BMP-TFSI leads to an increase of the surface dipole and thus to an increase of the work function by about 1.2 eV.

For the concomitant adsorption of Li and BMP-TFSI (Figure 3c), we find little change in the positions and structure of adsorbed Li and coadsorbed BMP-TFSI as compared to adsorption of the individual species. This in combination with the charge transfer from Li to C and the specific arrangement of cations and anions in the IL monolayer leads to a decrease in the work function relative to that of pristine graphite (0001). Compared with the individual adsorbates, the work function change is in between those of the two cases C–Li and C–IL, though closer to that of C–Li. Obviously, the positive charge on Li is maintained and dominates the work function change in the C–Li–IL system. Interestingly, the states of the IL seem to be pinned to the vacuum level in Figure 1,

which due to the decrease of the work function leads to a rigid shift of the electronic states of the IL to lower energies relative to the Fermi level and thus to an increase of their binding energy, as it had been mentioned for adsorbed ILs earlier.<sup>[35]</sup> Similar effects are expected for the core-level binding energies. Explicit calculations of core-level binding energies will be presented later.

Qualitatively, these values and trends in the calculated work function changes agree well with those in the experiment.<sup>[35]</sup> Quantitatively, however, the calculated work function change due to the adsorption of the IL in the monolayer structure (1.2 eV) is about 1 eV larger than the experimentally determined value of 0.2 eV.<sup>[35]</sup> This can at least partially be explained by temperature effects. As shown by an ab initio molecular dynamics simulation at 298 K (see Figure 4), the row-like structure of the BMP-TFSI monolayer<sup>[33]</sup> dissipates at that temperature. In particular, the large height difference between cations and anions vanishes, and after 10–16 ps, the difference in height of the N atoms in the BMP cations and in the TFSI anions is on average only about 0.5 Å. After 10–12 ps, the results derived from the AIMD simulations oscillate around rather constant mean values. In particular, the initial large height difference between cations and anions vanishes, and after 10–12 ps, the difference in the height of the N atoms in the BMP cations and in the TFSI anions is on average only about 0.5 Å. This thermalization is accompanied by a considerable decrease of the surface dipole and thus of the work function change. Eventually, the work function change reaches a mean value of about 0.6 eV, which is already considerably closer to the experimental value of 0.2 eV.<sup>[35]</sup>

### 2.2.2. Calculations of Core-Level Binding Energies of an Adsorbed BMP-TFSI Monolayer and of Reaction Products with Coadsorbed Li Atoms

Previously, we had shown that optimization of coadsorbed BMP-TFSI and Li on graphite (0001) leads to breaking of the

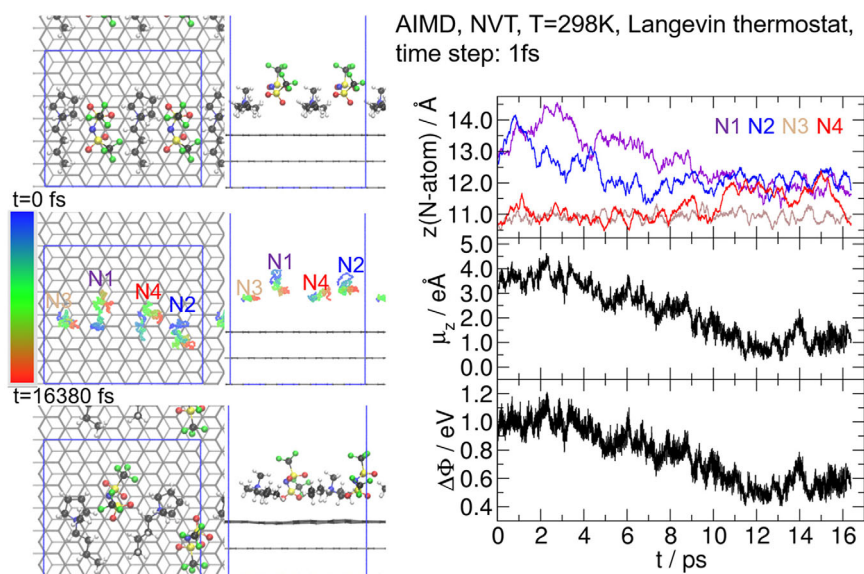


**Figure 4.** Changes of the structure (left panels and topmost right panel), the dipole moment normal to the surface ( $\mu_z$ ), and the work function ( $\Delta\phi$ ) in the BMP-TFSI monolayer on graphite (0001) during an AIMD simulation at 298 K.

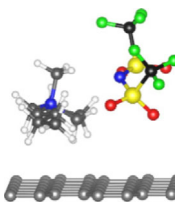
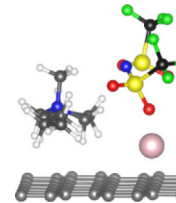
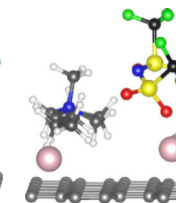
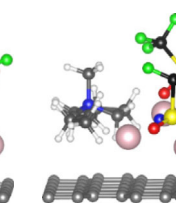
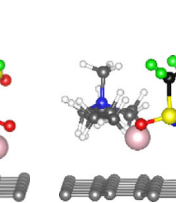
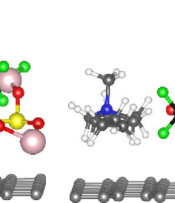
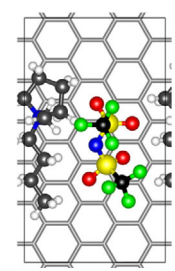
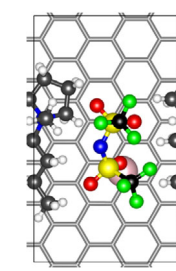
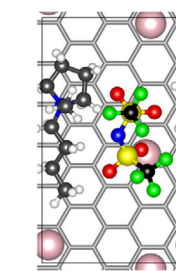
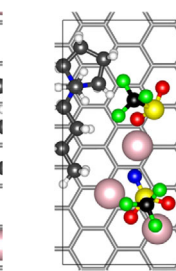
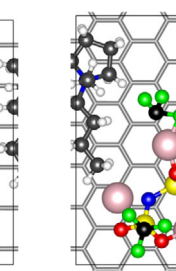
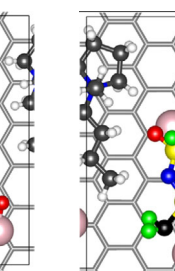


N—S bond in TFSI, and that this process is strongly exothermic if three Li atoms are present, while it would be endothermic or less exothermic for one or two Li atoms.<sup>[35]</sup> Interaction of Li with bulk BMP-TFSI was found to result in a spontaneous reaction of TFSI with Li in a nonactivated process, forming different reaction products such as  $\text{LiNSO}_2\text{CF}_3$ .<sup>[36]</sup> Here, N—S bond breaking was found to be about equally exothermic as S—C or C—F bond breaking.<sup>[36]</sup> These initial reaction products can decompose further via a sequence of activated steps. In the end, this was found to result in inorganic compounds composed of Li and the elements of TFSI such as  $\text{LiF}$ ,  $\text{Li}_2\text{O}$ ,  $\text{Li}_2\text{S}$ ,  $\text{LiCN}$ , or  $\text{LiCO}_3$  as the most stable reaction products, where the exact contributions depend on the chemical potential of Li, that is, on the amount of Li available.<sup>[36]</sup> At not-too-high chemical potentials, also  $\text{LiCO}_3$  and in particular  $\text{LiCN}$  were stable. In contrast, the reaction with BMP was found to be less facile. These results closely resemble previous findings in a DFT-MD study on the interaction of a TFSI containing IL,

*N*-butyl-*N*-methylpyrrolidinium (Pyr14)-TFSI, which at high excess of Li showed complete decomposition of the TFSI anions.<sup>[50]</sup>

In the present study, we want to elucidate the influence of the graphite (0001) substrate. We first calculated adsorption structures and core-level binding energies (BEs) of an adsorbed monolayer of BMP-TFSI on graphite (0001) and of adsorbed BMP-TFSI (in the same unit cell) coadsorbed with 1 or 3 Li species, where the latter can be considered as initial state after Li deposition on the BMP-TFSI monolayer covered graphite (0001) surface (see Table 2, 1st to 3rd column). Comparison of the calculated BEs with experimental ones shows the following trends: Postdeposition of Li is shown in Figure 1 to lead to an up-shift of the experimental core-level signals by about 1 eV, which agrees generally well with the trends in the calculated BEs. Exceptions are the F1s peak, where the shift is generally slightly smaller, both in the experiment and calculated, and the S2p peak, where in two of the calculated structures the shift is very small or even negative. This latter result is consistent with

**Table 2.** Topmost 2 rows: Top views and side views of the respective structures. Next two rows: Reaction energies  $\Delta E$  and  $\Delta E_2$  (in eV).  $\Delta E$  denotes the reaction energy with respect to adsorbed BMP-3Li-TFSI (3rd column);  $\Delta E_2$  denotes the reaction energy per Li atom with respect to BMP-TFSI and 3 isolated Li atoms. Further rows: N1s, F1s, O1s, C1s, and S2p represent core-level binding energies (in eV) for BMP-TFSI, BMP-Li-TFSI, BMP-3Li-TFSI, and the reaction products BMP- $\text{Li}_2\text{NSO}_2\text{CF}_3/\text{LiSO}_2\text{CF}_3$  (4th column), BMP- $\text{Li}_2\text{NSO}_2\text{CF}_3\text{SO}_2/\text{LiCF}_3$  (5th column), and BMP- $\text{Li}_2\text{NSO}_2\text{CF}_3\text{SO}_2\text{CF}_2/\text{LiF}$  (6th column) adsorbed on graphite (0001). Experimental core-level BEs of atoms of TFSI within the intact IL monolayer on graphite were used as reference for calibration against experiment and thus represent also the calculated BEs after calibration. For  $N_{\text{BMP}1s}$  (bottom row), this value represents the calculated BE after calibration.

Side view						
Top view						
$\Delta E$	–	–	–	– 4.91	– 4.52	– 4.79
$\Delta E_2$	–	–	–	– 3.33	– 3.20	– 3.29
N1s	399.5	400.4	400.5	398.4	399.4	400.1
F1s	689.1	689.6; 689.7	689.7	689.5	689.6 (SCF <sub>3</sub> ) 686.7 (CF <sub>3</sub> )	689.8 688.3 (CF <sub>2</sub> ) 687.5 685.8 (F)
O1s	532.8	534.0 534.5 (O—Li)	534.0	532.5; 532.9 533.3; 533.4 (NSO <sub>2</sub> CF <sub>3</sub> )	533.1 (NSO <sub>2</sub> ) 534.0	533.7 534.1
C1s	292.7	293.7	Not converged	292.5 (SO <sub>2</sub> CF <sub>3</sub> ) 293.0 (NSO <sub>2</sub> CF <sub>3</sub> )	289.9 (CF <sub>3</sub> ) 293.4	289.0 (CF <sub>2</sub> ) 293.3 (NSO <sub>2</sub> CF <sub>3</sub> )
S2p	168.9	170.7 169.8 (S—O—Li)	169.8	166.6 (SO <sub>2</sub> CF <sub>3</sub> ) 168.8 (NSO <sub>2</sub> CF <sub>3</sub> )	167.1 (SO <sub>2</sub> NSO <sub>2</sub> CF <sub>3</sub> ) 169.5 (NSO <sub>2</sub> CF <sub>3</sub> )	169.6 (NSO <sub>2</sub> CF <sub>3</sub> )
$N_{\text{BMP}1s}$	402.7	403.8	404.0	403.7	403.9	404.0



experimental findings, when considering also the lower BE peak fitted into the doublet at about 170 eV. Hence, the up-shift of the peaks in the spectra recorded upon Li postdeposition can be assigned to chemical effects resulting from the coadsorption of Li with BMP-TFSI as shown in Table 2 or to the formation of initial reaction products with a largely intact molecular structure. Comparison of these results with those reported recently for reaction between thick BMP-TFSI multilayers and Li<sup>[36]</sup> shows rather similar trends, with the exception that the up-shift upon Li postdeposition is smaller in that case than for the adsorbed BMP-TFSI monolayer. This can be reconciled by the fact that due to the vacuum level pinning in the multilayer system its BEs were already up-shifted compared to the monolayer.<sup>[36]</sup> Hence, in that case, the BEs are less affected by initial interaction with Li, as long as the molecular structure of the ion pairs is largely intact.

In the next step, we explored the adsorption structures, reaction energies, and core-level binding energies of the most relevant initial reaction products between adsorbed BMP-TFSI and 3 Li atoms coadsorbed at a monolayer coverage of the IL on the graphite (0001) surface. Considering that in our previous calculations on the reaction of bulk BMP-TFSI with Li (see Figure 5d–f in ref. [36]), Li-induced N–S bond breaking was found to be highly exothermic and to proceed spontaneously with no activation barrier,<sup>[36]</sup> and similar results were obtained also for Li-induced S–C or C–F bond breaking. Therefore, we decided to focus on these reactions also for the adsorbed monolayer. As illustrated in Table 2 (4th to 6th column), these reactions are strongly exothermic also in the present case. Formation of a Li<sub>2</sub>-NSO<sub>2</sub>CF<sub>3</sub> intermediate (N–S bond breaking) seemed to be most likely, although intermediates with broken S–C or C–F bonds are only slightly less stable and thus their formation may be possible as well (Table 2, 4th to 6th column). Finally, although not calculated explicitly for the monolayer case, we expect that similar to the reaction of Li with bulk BMP-TFSI the reaction proceeds spontaneously, with no or only a small activation barrier.<sup>[36]</sup>

For further information, we compare the calculated core-level BEs of the coadsorbed species and of the three adsorbed initial reaction products (Table 2) with the experimental data. For this purpose, the calculated BEs are indicated by symbols in Figure 1 at the top of the different panels (symbols are explained in the legend in the figure). For the F1s region, most of the adsorbed molecular species are in the range of the F<sub>TFSI+Li</sub> peak. Also, the difference in BE between F<sub>TFSI+Li</sub> and F<sub>TFSI</sub> peaks is reproduced well. The products in the 5th and 6th rows show also signals at significantly lower BE, at 686.7 eV (5th row: S–C bond breaking) and at 685.8 eV (6th row: C–F bond breaking), respectively, in addition to signals at higher BE. Unfortunately, these latter signals are close to the low BE peak (F<sub>TFSI,dec-1</sub>) in the experimental spectra in Figure 1. Therefore, they may also be due to a later reaction product such as LiF (see discussion below), and an unambiguous confirmation or exclusion of these latter species is not possible based on their BEs. For the O1s region, the situation is so far different as the BE of the low-BE peak is only reproduced by the binary adsorbates (see below), while all other species show BEs in the range of the high-BE peak (O<sub>TFSI+Li</sub> and O<sub>TFSI,dec-1</sub>). Also in this case, the up-shift in BE upon Li coadsorption, from the O<sub>TFSI</sub> to the O<sub>TFSI+Li</sub> peak, is reproduced well. A similar situation

is obtained for the S2p region, where all adsorbed molecular species, both the initial IL and the initial reaction products, appear in the BE range of the high-BE peaks (S<sub>TFSI+Li</sub> and S<sub>TFSI,dec-1</sub>). Also, the up-shift in BE upon coadsorption of Li, from S<sub>TFSI</sub> to S<sub>TFSI+Li</sub>, is again well reproduced. Finally, similar to the O1s state, the BE of the low-BE S<sub>TFSI,dec-2</sub> peak is only reproduced by the binary adsorbed species (Li<sub>3</sub>S, Li<sub>4</sub>S, see below).

Most complex is the situation for the N1s region. To begin with, the up-shift of the BE from the N<sub>BMP</sub> and N<sub>TFSI</sub> peaks to the related N<sub>BMP+Li</sub> and N<sub>TFSI+Li</sub> peaks is again well reproduced. The adsorbed molecular species resulting from the interaction of BMP and Li are very close to the BE of the coadsorbed BMP-Li-TFSI and BMP-Li-TFSI species. For the TFSI-related decomposition products, the BEs are more spread out. While one of them (BMP-LiNSO<sub>2</sub>CF<sub>3</sub>SO<sub>2</sub>CF<sub>2</sub>/F) shows a N1s BE close to that of the coadsorbed TFSI + Li species, the other two exhibit BEs close to the low-BE N<sub>TFSI,dec-2</sub> peak (BMP-Li<sub>2</sub>NSO<sub>2</sub>CF<sub>3</sub>/LiSO<sub>2</sub>CF<sub>3</sub>) or in between the two signals (BMP-Li<sub>2</sub>NSO<sub>2</sub>CF<sub>3</sub>SO<sub>2</sub>/LiCF<sub>3</sub>). Nevertheless, it is not possible to exclude one of the initial reaction products in Table 2 by comparison with the experimental peaks and their BEs. Finally, for the C1s region, the overlap with the graphite-related signals precludes a detailed comparison between calculated and experimental BEs. In total, within the accuracy of the calculated BEs, it is not possible to exclude any one of the three initial reaction products based on the experimental XPS spectra in Figure 1. Most likely, these reactions proceed in a competitive way, and we see coexistent signals with BEs typical for all three initial reaction products, in addition to those of the coadsorbed BMP-TFSI + Li species. Most of the subsequent reaction steps seem to be activated, as concluded from the higher reaction temperatures required for the activation of these steps. The low-BE signals characteristic for the binary adsorbed species are mostly formed upon annealing.

Based on these calculations, the initial reactions between adsorbed BMP-TFSI and coadsorbed Li seem to proceed via similar reaction pathways as deduced for the reaction between bulk BMP-TFSI and Li. The close similarity between reactions between the adsorbed BMP-TFSI monolayer and coadsorbed Li on the one hand and between bulk BMP-TFSI and Li on the other hand can be rationalized by the predominantly nonchemical interaction between BMP-TFSI and the graphite (0001) surface and the resulting little change in the electronic properties of BMP-TFSI upon adsorption on the graphite surface. Furthermore, the different charge state of the initial Li reactant, once a Li<sup>0</sup> atom (in the bulk reaction) and once a positively charged adsorbed Li<sup>δ+</sup> species, does not seem to significantly modify the reaction pathway.

Finally, we will focus on the thermodynamically stable final products of the reaction of BMP-TFSI and Li. For reaction with bulk BMP-TFSI, equivalent to the multilayer film, we found the binary salts composed of Li and elements of TFSI such as Li<sub>2</sub>O, LiF, Li<sub>3</sub>N, Li<sub>2</sub>S, or LiCN to be the most stable.<sup>[36]</sup> Similar type results were reported from a DFT-based molecular dynamics study on the interaction of the closely related pyrrolidinium (Pyr) based ionic liquid Pyr-TFSI with Li by Merinov et al. who found complete decomposition of TFSI in the presence of a large excess of Li.<sup>[50]</sup> In their work, F atoms were typically coordinated by 4 or 3 Li atoms. Comparable results were reported also in an earlier DFT-based

molecular dynamics study by Yildirim and Haskins et al.<sup>[51,52]</sup> who explored decomposition reactions and products at the Li-ionic liquid interface, but without reaching fully equilibrated atomistic structures of the interface.

In order to verify whether such products could be formed in our experiments on the graphite surface, we calculated optimized structures for adsorbed  $\text{Li}_n\text{X}$  clusters on the surface (see Table 3), followed by calculations of the core-level binding energies. The choice of these species was based on the previous report by Merinov et al. that in the presence of excess Li, the anion F is three- or fourfold coordinated.<sup>[50]</sup> Furthermore, higher coordination of the anions, either fourfold ( $\text{Li}_2\text{O}$ ,<sup>[53]</sup>  $\text{Li}_2\text{S}$ ,<sup>[53]</sup> or  $\text{LiCN}$ <sup>[54]</sup>), sixfold ( $\text{LiF}$ <sup>[55]</sup>), or eightfold ( $\text{Li}_3\text{N}$ <sup>[56]</sup>) coordination, is present also in the respective bulk structures. The resulting most stable structures are summarized in Table 3.

In general, there is little difference in the BEs calculated for the adsorbed  $\text{Li}_3\text{X}$  and  $\text{Li}_4\text{X}$  species, indicating that the charge donated by the additional Li is largely transferred to the graphite substrate. Exceptions are the N1s and S2p levels in  $\text{Li}_3\text{N}$  and  $\text{Li}_3\text{S}$ , respectively, where the differences in BE are about 1 eV. Furthermore, the BEs calculated for these structures closely resemble those obtained in recent calculations of anions X in the respective bulk structures,<sup>[36]</sup> indicating that the interaction with graphite has little influence on the core-level BEs of these species as compared to the respective bulk environment. Only for LiF we find a significant difference. Most likely, this discrepancy is due to the failure of the GGA functional to accurately describe the position of the valence band of such systems with large band gaps.<sup>[36,57]</sup> Hence, we are convinced that the assignment of the  $\text{F}_{\text{TFSI,dec-1}}$  peak to an adsorbed  $\text{LiF}_x$  species is justified.

For comparison with the experimental spectra, we also included the calculated BEs of the  $\text{Li}_3\text{X}$  and  $\text{Li}_4\text{X}$  species as colored symbols in Figure 1, similar to the approach for the coadsorbed species and initial reaction products discussed before. The calculated BEs generally agree quite well with the BEs of the low-BE peaks formed during postdeposition of Li and in particular during

the annealing sequence. It should be noted, however, that the correlation is not unique, in the sense that for some states such as F1s or N1s also a molecular species ( $\text{BMP-Li}_2\text{NSO}_2\text{CF}_3\text{SO}_2/\text{LiCF}_3$ ) shows a signal in the low BE range, while for the O1s and S2p signals only the binary compound feature signals in this BE range. Hence, in these cases, we can unambiguously conclude on the presence of these adsorbed binary components once these low-BE peaks appear. Furthermore, for the  $\text{Li}_3\text{N}$  species, we obtained a very low N1s signal with a BE of only 393.9 eV ( $\text{Li}_3\text{N}$ ) or 394.8 eV ( $\text{Li}_3\text{N}$ ), which is well below the low BE  $\text{N}_{\text{TFSI,dec-2}}$  peak in the spectra at 398.9 eV (Figure 1). Based on this discrepancy and from the fact that adsorbed LiCN shows a calculated N1s signal at 399.0 eV (Table 3), we postulate that the binary compound in the low-BE peak ( $\text{N}_{\text{TFSI,dec-2}}$ ) is related to the formation of LiCN rather than of  $\text{Li}_3\text{N}$ . We are convinced that this assignment is conclusive, despite the lack of direct experimental evidence.

Similar observations were also made for the Li-induced reactive decomposition of thick BMP-TFSI films. The BEs of initial BMP-TFSI reaction products corresponding to those in the monolayer system and of the binary compounds appearing upon Li post-deposition are indicated at the top of the respective panels in Figure 2. Also in this case, Li postdeposition leads to XP spectra that are consistent with the calculated BEs of the initial reaction products (high-BE components) and, in particular after subsequent annealing, of the binary compounds (low-BE components). BEs of further possible bulk reaction intermediates were listed in our previous study.<sup>[36]</sup> The high-BE components are compatible with all three initial reactions (N–S, S–C, C–F bond breaking), very similar to the trends observed for the reaction of Li with the monolayer film. This agreement further supports our earlier conclusion that the presence of the graphite substrate does not severely modify the pathway for the reactive, Li-induced decomposition of BMP-TFSI. Although we have no direct proof for this assumption, we assume that also subsequent reaction intermediates formed by further reaction of the initial reaction products (Table 2), until finally arriving at the binary compounds listed in Table 3, are identical in both cases.

Furthermore, the data indicate that while the initial reaction between adsorbed BMP-TFSI, and in particular between TFSI and Li, is little activated or spontaneous and proceeds already at RT, complete Li-induced decomposition of the BMP-TFSI-like molecular fragments is highly activated and requires significant annealing. Depending on the final product, the required annealing temperatures vary between >400 K for N-containing species, >500 K for F-containing species, and 650 K for S- or O-containing species. The activation barriers are even higher for removal of the resulting adsorbed binary compounds, reaching 650 K for LiF- and LiCN-like adsorbates and >650 K for  $\text{Li}_2\text{S}$ - and  $\text{Li}_2\text{O}$ -like adsorbed species (Figure 1), and rather similar barriers are obtained also for reaction with a thick BMP-TFSI film (Figure 2). Accordingly, for the reaction of a monolayer of BMP-TFSI and coadsorbed Li at RT one would expect a kinetically controlled, complex mixture between remaining BMP-TFSI-like species (coadsorbed with Li, as indicated in Table 2), the initial reaction products as indicated in Table 2, molecular reaction intermediates resulting from the stepwise Li-induced further

**Table 3.** N1s, O1s, F1s, C1s, and S2p core-level binding energies (in eV) for the stable structures of  $\text{Li}_n\text{X}$  (X = N, O, F, S, CN) adsorbates on graphite (0001).

		$\text{Li}_3\text{X}$		$\text{Li}_4\text{X}$	
X	Core level	BE in bulk $\text{LiX}/\text{Li}_2\text{X}/\text{Li}_3\text{X}$ <sup>[36]</sup>	BE in $\text{Li}_3\text{X}$	BE in $\text{Li}_4\text{X}$	
N	N1s	394.3/395.2	393.9	394.8	
O	O1s	529.8	529.6	530.2	
F	F1s	684.9/685.0	687.2	687.8	
S	S2p	160.8	160.6	161.5	
CN	N1s	398.4	399.0 (LiCN)	–	
–	C1s	285.6	285.8 (LiCN)	–	

decomposition of the species, and finally contributions from the different binary adsorbed species (Table 3). The same is true also for the reaction between bulk BMP-TFSI and Li. This also means that under such conditions the exact product composition will depend sensitively on the reaction parameters.

### 2.3. Relevance of such Kind of Model Studies for the Understanding of SEI Formation in a Realistic Battery Environment

Clearly, the results presented and discussed above were obtained using strongly simplified model systems in an idealized environment, leading to questions about the relevance of such model studies for the understanding of SEI formation in a realistic battery environment. For this purpose, we will first compare the present results with observations reported for a realistic, electrochemical environment. Generally, it is expected that the SEI formation starts in the first potential cycle once the anode potential falls below the electrolyte reduction potential.<sup>[2,15,25,26]</sup> This is, however, a purely electrochemical picture based on electron transfer, which does not consider chemical interactions between electrode and solvent/electrolyte. Thus, depending on the chemical reactivity of the electrode surface, decomposition of the solvent by chemical reactions may start also much earlier, and possibly even spontaneously. While such kinds of chemical interactions with the surface seem to be unlikely in the present case of a graphite electrode, they can become important for more reactive electrode materials. Model studies like the present one therefore provide access to these chemical interactions and their impact on SEI formation.

The results discussed before had shown that at least part of these chemical reactions is activated with a significant activation barrier, which can be overcome only by some kind of activation. This may be by thermal activation, as in the present case, by reducing the barrier via the application of a potential difference between electrode and electrolyte or by other ways. In that picture, the resulting products and thus the composition of the initial SEI depend on the extent of activation, as indicated by the different compositions of the adlayer after annealing to increasing temperatures. Previous studies of SEI formation in BMP-TFSI-based electrolytes had shown that mainly inorganic binary compounds, in particular LiF, were present in the range close to the electrode–SEI interface, reflecting complete decomposition of the TFSI.<sup>[41]</sup> In contrast, the range further away from that interface was increasingly dominated by organic species, indicating incomplete decomposition of the TFSI. This structure must be due to a change in experimental conditions with increasing SEI thickness, for example, in the chemical activity of the surface of the growing SEI or in the local concentration of different species during the SEI formation process. Alternatively, it could be caused by a change in the local potential due to a potential drop over the SEI, leading to a change in electrochemical activation of the decomposition process, which becomes less effective with increasing thickness of the SEI and thus decreasing potential difference between SEI and electrolyte. In total, we propose a more chemical picture of the SEI formation than models based on electron transfer-induced reduction of the electrolyte, as already suggested for

other systems,<sup>[24]</sup> and model studies like the present one can lead to a comprehensive understanding of the chemical reactions going on during SEI formation.

Next, we would like to comment on the apparent difference between the present model study, where Li was deposited as metallic Li<sup>0</sup> species, and the situation in an electrochemical cell, where Li is deposited as Li<sup>+</sup> ion. For the reaction between the BMP-TFSI monolayer and coadsorbed Li, it is likely that there is no difference, since in this case, the reaction may start from coadsorbed species, where it does not matter whether Li arrived initially as neutral Li<sup>0</sup> or as ionic Li<sup>+</sup> species. This is different for reaction with the thick BMP-TFSI film, where reaction with Li<sup>0</sup> can result in an initial electron transfer into the LUMO of TFSI, which is not possible for reaction with Li<sup>+</sup>. In that case, Li<sup>0</sup> provides the electron for the reduction of BMP-TFSI which otherwise would come from the electrode. The present experimental and theoretical results show the formation of rather similar products for the reaction of coadsorbed Li with the adsorbed BMP-TFSI monolayer and for the reaction of Li with a thick multilayer film, equivalent to bulk TFSI. This seems to indicate that the difference in the oxidation state of the incoming Li is not decisive, at least not for the present system. Other differences between the present model system and the realistic electrochemical environment such as the formation of solvent shells are, however, not included and need to be considered in a more detailed approach.

Finally, we would like to briefly comment on future developments for an improved XPS analysis of complex surfaces such as SEI layers. In that case, the identification of possible reaction products should involve an analysis not only of the binding energies (BEs) of the different species, but also of the relative intensities of the related peaks. These should reflect the stoichiometric composition of the different products after correction by the ASFs of the different signals. Furthermore, also effects caused by the different mean free paths of the different signals have to be considered in such kind of analysis. Because of the large number of possible reaction products, this is an enormous effort that was out of reach in the present work. Nevertheless, this should be tackled in the future, perhaps by using AI-based concepts.

## 3. Conclusions

Aiming at a molecular-scale understanding of the chemical processes leading to the formation of the solid–electrolyte interphase in Li-ion batteries, we have investigated the reaction between an adsorbed monolayer of the ionic liquid BMP-TFSI and Li on a graphite (0001) surface on the one hand and, for comparison, between a thick, bulk-like film of BMP-TFSI and Li on the other hand. Combining results from experiment, from XPS measurements after Li postdeposition and annealing to increasing temperatures, and from theory including reaction energies, charge transfer/dipole moments/changes in work function, and core-level binding energies, we arrive at the following conclusions: 1) Adsorption of BMP-TFSI on graphite (0001) leads to an increase in the work function due to the different heights of the adsorbed cations and anions, which in total leads to an

increase in the surface dipole. The much higher calculated increase of the work function (+1.2 eV) as compared to the experimental value of 0.2 eV can be rationalized by a thermally induced breakdown of the ordered adlayer at 298 K, which leads to a lower average position of the anions and thus to a significantly smaller surface dipole and work function increase. Adsorption is dominated by nonchemical interactions. 2) Coadsorption of one BMP-TFSI ion pair and one Li leads to a slight decrease of the surface dipole and thus of the work function. The charges on the different species, adsorbed BMP, adsorbed TFSI, and adsorbed Li, largely resemble those obtained for the individual adsorbates BMP-TFSI and Li. 3) For the initial reaction between adsorbed BMP-TFSI and coadsorbed Li, Li-induced N—S, S—C, or C—F bond-breaking reactions are highly exothermic and therefore thermodynamically favorable. Based on their characteristic core-level signals, these reactions can proceed during Li postdeposition on the BMP-TFSI monolayer film at RT, indicative of a weakly or even nonactivated process. Considering the small energy differences between the different reaction products, and assuming low barriers, the different initial reaction products will form simultaneously and coexist. Interaction with Li during postdeposition at 300 K also leads to the formation of F- and C-containing volatile decomposition products, in addition to solid adsorbed species. Further decomposition up to binary  $X_3\text{Li}$ - or  $X_4\text{Li}$ -like adsorbed species ( $X = \text{F}, \text{O}, \text{S}, \text{CN}$ ) is possible, but at least part of the reaction steps involved is highly activated, as evidenced by the fact that complete decomposition into these species is possible only upon annealing to 650 K. 4) Similar reaction products are obtained also for the reaction between Li and bulk BMP-TFSI, and also in that case, the barriers estimated from the annealing steps are generally of comparable magnitude, though not always. Complete conversion into binary compounds requires annealing to temperatures comparable to those in the monolayer case. BEs calculated for the resulting products are compatible with those observed in the measured XP spectra. 5) Based on the close similarity between the Li-induced decomposition of a preadsorbed BMP-TFSI monolayer film with the reaction between a multilayer bulk-like BMP-TFSI film and postdeposited Li, the nonchemical interaction between the graphite substrate and BMP-TFSI has no significant impact on the reaction with Li. The same seems to be true also for the difference in the initial state of Li: postdeposited Li can coadsorb and transfer electron charge to the graphite substrate to form  $\text{Li}^{\delta+}$  in the monolayer case, while during interaction with bulk BMP-TFSI charge is directly transferred to the ionic liquid ions. 6) In the range of Li:N ratios covered in this study, the formation of  $\text{Li}_3\text{N}$  can be ruled out based on the N1s binding energies. Instead,  $\text{LiCN}$  formation seems to be more favorable, consistent also with the computational results. 7) Comparison of the chemical decomposition behavior of BMP-TFSI investigated here with that in a realistic battery environment, where binary compounds such as  $\text{LiF}$  are formed already at RT in deeper layers, closer to the anode–SEI interface, and dominate the SEI in that region, indicates that the insufficient thermal activation of the decomposition reactions can partly be compensated by electrochemical activation. Assuming a potential drop over the SEI, this can be explained by the larger potential difference between anode and electrolyte

at the beginning of the SEI formation, while with increasing SEI formation this is replaced by the decreasing potential difference between SEI surface and electrolyte. In consequence, complete decomposition into the binary compounds is no longer possible, and molecular fragments prevail in the outer regions of the SEI.

Overall, we have shown that combined experimental and theoretical model studies, using structurally well-defined electrodes as well as an equally well-defined, simplified environment, in this case ultrahigh vacuum, can provide detailed insights into the complex molecular scale processes during the initial stages of SEI formation. They allow us to separate chemical and electrochemical effects and provide information on the role of the electrode surface in the underlying electrolyte decomposition processes. These are key ingredients for a systematic, knowledge-based development of electrolytes with improved stabilities and SEI formation, and thus indispensable for the development of improved future battery systems.

## 4. Experimental Section

### Experimental

The XPS measurements were carried out in a commercial UHV system (SPECS) with a background pressure of around  $2 \times 10^{-10}$  mbar, which among others was equipped with an X-ray source (SPECS XR50, Al- $K_{\alpha}$  and Mg- $K_{\alpha}$ ) and a hemispherical analyzer (SPECS, DLSEGD-Phoibos-Has3500). We used nonmonochromatized Al- $K_{\alpha}$  radiation (1486.6 eV) with the X-ray gun operated at a power of 250 W ( $U = 14$  kV,  $I = 17.8$  mA). The XP spectra were recorded at a pass energy  $E_{\text{pass}}$  of 100 eV at grazing emission ( $80^\circ$  to the surface normal, surface sensitive mode). For the quantitative analysis of the XP spectra, fitting of the peaks was performed using the Igor pro 8.04 software with a simultaneous fit of the background (Shirley + slope) and signal, assuming a pseudo-Voigt type peak shape, which is a linear combination of a Gaussian and a Lorentzian function. Atomic sensitivity factors (ASFs) for our set-up for the different spectral regions were evaluated using a molecularly adsorbed BMP-TFSI ( $\text{C}_{11}\text{H}_2\text{OF}_6\text{N}_2\text{O}_4\text{S}_2$ ) multilayer film on the graphite (0001) substrate, where the ASF for F1s is set to 1, which leads to ASFs for C1s: 0.21, O1s: 0.57, S2p: 0.40 and N1s: 0.35.<sup>[40]</sup>

The highly oriented pyrolytic graphite (0001) (HOPG) substrate was purchased from MaTeck (ZYA, mosaic spread  $0.4^\circ \pm 0.1^\circ$ , size of  $10 \text{ mm} \times 10 \text{ mm} \times <1 \text{ mm}$ ). Before transferring the HOPG into the load lock of the UHV system, it was fixed on a tantalum sample plate with conductive silver paste, heated in a  $\text{N}_2$  flooded oven for 30 min at 720 K to degas the silver paste, and then freshly cleaved. Afterward, it was transferred from the load lock into the UHV chamber and flashed to  $\approx 600$  K to generate a clean graphite (0001) surface. The sample temperature in the main UHV chamber was measured via a pyrometer (LumaSense Technologies, IP 140). Samples were slowly heated up over a few minutes, using a filament below the sample (0.8–1.8 A), until the desired temperature was reached. Here the temperature was held for about 1 min, before it was allowed to cool down again. For higher temperatures, we applied a voltage (50–130 V) between filament and sample. XPS measurements were conducted after the described heating procedure was finished. The ionic liquid (IL) 1-butyl-1-methylpyrrolidinium bis(trifluoromethylsulfonyl)imide (BMP-TFSI) was filled into a quartz crucible, which was mounted in a Knudsen effusion cell (Ventiotec, OVD-3). To generate a pure, water-free IL, it was first degassed in the load lock system at around 400 K. Subsequently, the IL source was heated up in



the main UHV chamber to the IL evaporation temperature of 450 K, where evaporation started, but with a negligible increase of the base pressure. Under these conditions, the IL deposition rate was  $\approx 0.1 \text{ ML min}^{-1}$ , with 1 monolayer (ML) defined as a layer at saturation coverage in the first layer (approx. layer thickness  $d$ : 3.5 Å).

Lithium metal was deposited from an alkali getter source (SAES Getters) by resistively heating the source (7.1 A, 1.1 V) in line-of-sight of the sample at a distance of around 6 cm. Under these conditions, the Li deposition rate was around  $0.04\text{--}0.05 \text{ ML min}^{-1}$ , where a monolayer corresponds to a saturated Li layer with a Li layer thickness  $d$  of  $\approx 2.5 \text{ Å}$ .<sup>[34]</sup> The layer thicknesses  $d$  were calculated using the relation  $d = -\ln(I_d/I_0) \times (\lambda \cos \theta)$  ( $I_0$ : substrate peak intensity before deposition,  $I_d$ : intensity after deposition,  $\lambda$ : the inelastic mean free path (IMFP) in the film material at the given electron energy,  $\theta$ : emission angle with respect to the surface normal), assuming a homogeneous layer by layer growth. Here, we used electron inelastic mean free paths (IMFPs)  $\lambda$  of 46 Å in Li<sup>[58]</sup> and of 35 Å in the IL<sup>[59]</sup> at kinetic energies of  $\approx 1200 \text{ eV}$  (C1s graphite peak) for the calibration of the deposited amounts of Li and IL.<sup>[46]</sup> The latter signal was also used to calibrate the binding energy (BE) scale.

## Computation

We employed periodic DFT calculations as implemented in the Vienna ab initio simulation package (VASP 5.4)<sup>[60,61]</sup> to study the interactions and possible reactions of a BMP-TFSI monolayer with Li atoms at the graphite (0001) surface. The revised Perdew–Burke–Ernzerhof functional (RPBE) was used to describe the electronic exchange and correlation effects.<sup>[62]</sup> Additionally, semiempirical dispersion corrections (D3) were taken into account.<sup>[63]</sup> Ionic cores were represented by the projected augmented wave method (PAW).<sup>[64,65]</sup> The electronic wave functions were expanded in a plane wave basis set, employing an energy cutoff of 520 eV. The electronic structure was converged within  $10^{-6} \text{ eV}$ . Geometries were optimized until all forces on atoms were less than  $0.01 \text{ eV Å}^{-1}$ .

The graphite (0001) surface was represented by a slab consisting of three graphene layers. A vacuum region of about 23 Å was inserted between the surface slabs. A rectangular surface unit cell with the dimensions ( $8.581 \text{ Å} \times 14.863 \text{ Å}$ ) containing one IL pair, which was based on experimental STM images reported previously,<sup>[33]</sup> was employed as model for the overlayer structure. The integration over the first Brillouin zone was done employing a  $2 \times 1 \times 1$  gamma-centered k-point mesh.

Core-level binding energies (BE) were calculated employing the implementation in VASP developed by Köhler and Kresse.<sup>[66]</sup> According to this approach, the BE is related to the total energy difference between a final state in which the electron of the respective core level is excited into the valence states and the initial ground state. For the calculation of the final states, the remaining core electrons are kept frozen within the pseudopotential, while the valence electrons are allowed to relax. For direct comparison to the experiment, calculated BEs of the different core levels  $X$  ( $\text{BE}_{\text{calc}}(X)$ ) were calibrated, using the experimental and calculated values of core-level BEs of intact TFSI adsorbed on HOPG at a monolayer coverage of BMP-TFSI<sup>[33]</sup> as reference

$$\text{BE}(X) = \text{BE}_{\text{calc}}(X) + \text{BE}_{\text{exp}}(X_{\text{TFSI}}) - \text{BE}_{\text{calc}}(X_{\text{TFSI}}) \quad (1)$$

where  $X$  or  $X_{\text{TFSI}}$  denote the N1s, C1s, F1s, O1s, or S2p levels in the respective adsorbate ( $X$ ) or in TFSI ( $X_{\text{TFSI}}$ ). We also tested whether the size of the unit cell has an impact on the calculated BE and found that doubling the surface unit cell along the shortest lattice vector (lattice vector  $a$ ) only leads to small changes in the calculated BEs. For example, the BE(N1s) of the decomposition product of TFSI with a broken

N—S bond changes only by about 0.1 eV if the surface unit cell doubles.

AIMD simulations of the BMP-TFSI monolayer structure on graphite were performed to identify changes in the work function due to a temperature-induced movement of the ions. In these simulations, we employed a canonical (NVT-) ensemble with a Langevin thermostat at a temperature of 298 K and time steps of 1 fs. In order to allow a better reorganization of the adsorbed ions, the unit cell was doubled along the lattice vector  $a$ , and the total run time of the AIMD simulation was 16.4 ps.

## Acknowledgements

The authors gratefully acknowledge financial support from the German Research Foundation (DFG) under project ID 390874152 (POLiS Cluster of Excellence, EXC 2154) and computer time provided by the state of Baden-Württemberg through bwHPC and the DFG through grant no. INST 40/575-1 FUGG (JUSTUS 2 cluster). The work contributes to the research performed at CELEST (Center for Electrochemical Energy Storage Ulm-Karlsruhe).

Open Access funding enabled and organized by Projekt DEAL.

## Conflict of Interest

The authors declare no conflict of interest.

## Author Contributions

**Katrin Forster-Tonigold:** conceptualization (equal); data curation (equal); formal analysis (equal); investigation (equal); writing—original draft (equal); writing—review & editing (equal).

**Florian Buchner:** conceptualization (equal); data curation (equal); investigation (equal); validation (equal); visualization (equal); writing—review & editing (equal). **Axel Groß:** conceptualization (supporting); funding acquisition (lead); writing—review & editing (equal). **R. Jürgen Behm:** conceptualization (equal); supervision (equal); writing—original draft (equal); writing—review & editing (equal).

## Data Availability Statement

The data that support the findings of this study are openly available in Zenodo at <https://doi.org/10.5281/zenodo.15064332>.

**Keywords:** density functional calculations · ionic liquids · lithium · solid–electrolyte interactions · X-Ray photoelectron spectroscopy

- [1] D. Aurbach, B. Markovsky, G. Salitra, E. Markevich, Y. Talyossef, M. Koltypin, L. Nazar, B. Ellis, D. Kovacheva, *J. Power Sources* **2007**, *165*, 491.
- [2] J. B. Goodenough, Y. Kim, *Chem. Mater.* **2010**, *22*, 587.
- [3] S. K. Heiskanen, J. Kim, B. L. Lucht, *Joule* **2019**, *3*, 2322.
- [4] E. Peled, *J. Electrochem. Soc.* **1979**, *126*, 2047.
- [5] E. Peled, D. Golodnitsky, G. Ardel, *J. Electrochem. Soc.* **1997**, *144*, L208.
- [6] K. Xu, *Chem. Rev.* **2004**, *104*, 4303.

- [7] J. Vetter, P. Novak, M. R. Wagner, C. Veit, K. C. Müller, J. O. Besenhard, M. Winter, M. Wohlfahrt-Mehrens, C. Vogler, A. Hammouche, *J. Power Sources* **2005**, *147*, 269.
- [8] M. Winter, *Z. Phys. Chem.* **2009**, *223*, 1395.
- [9] P. Verma, P. Maire, P. Novák, *Electrochim. Acta* **2010**, *55*, 6332.
- [10] M. Gauthier, T. J. Carney, A. Grimaud, L. Giordano, N. Pour, H. H. Chang, D. P. Fenning, S. F. Lux, O. Paschos, C. Bauer, M. Filippo, S. Lupart, P. Lamp, Y. Shao-Horn, *J. Phys. Chem. Lett.* **2015**, *6*, 4653.
- [11] S. J. An, J. Li, C. Daniel, D. Mohanty, S. Nagpure, *Carbon* **2016**, *105*, 52.
- [12] E. Peled, S. Menkin, *J. Electrochem. Soc.* **2017**, *164*, A1703.
- [13] V. A. Agubra, J. W. Fergus, *J. Power Sources* **2014**, *268*, 153.
- [14] K. Xu, *Chem. Rev.* **2014**, *114*, 11503.
- [15] A. Wang, S. Kadam, H. Li, S. Shi, Y. Qi, *npj Comput. Mater.* **2018**, *4*, 15.
- [16] K. Kwon, F. Kong, F. McLarnon, J. W. Evans, *J. Electrochem. Soc.* **2003**, *150*, A229.
- [17] G. M. A. Girard, M. Hilder, N. Dupre, D. Guyomard, D. Nucciarone, K. Whitbread, S. Zavorine, M. Moser, M. Forsyth, D. R. MacFarlane, P. C. Howlett, *ACS Appl. Mater. Interfaces* **2018**, *10*, 6719.
- [18] L. Cabo-Fernandez, D. Bresser, F. Braga, S. Passerini, L. J. Hardwick, *Batteries Supercaps* **2019**, *2*, 168.
- [19] J. Maibach, L. Källquist, M. Andersson, S. Urpelainen, K. Edström, H. Rensmo, H. Siegbahn, M. Hahlin, *Nat. Commun.* **2019**, *10*, 3080.
- [20] J. Maibach, J. Rizell, A. Matic, N. Mozhzhukhina, *ACS Mater. Lett.* **2023**, *5*, 2431.
- [21] D. Schäfer, K. Hankins, M. Allion, U. Krewer, F. Karcher, L. Derr, R. Schuster, J. Maibach, S. Mück, D. Kramer, R. Mönig, F. Jeschull, S. Daboss, T. Philipp, G. Neusser, J. Romer, K. Palanisamy, C. Kranz, F. Buchner, R. J. Behm, A. Ahmadian, C. Kübel, I. Mohammad, A. Samoson, R. Witter, B. Smarsly, M. Rohnke, *Adv. Energy Mater.* **2024**, *14*, 2302830.
- [22] H. S. Dhattarwal, Y. W. Chen, J. L. Kuo, H. K. Kashyap, *J. Chem. Phys. C* **2020**, *124*, 27495.
- [23] J. Han, H. Euchner, M. Kuenzel, S. M. Hosseini, A. Groß, A. Varzi, S. Passerini, *ACS Energy Lett.* **2021**, *6*, 3063.
- [24] D. Stottmeister, A. Groß, *Batteries Supercaps* **2023**, *6*, e202300156.
- [25] B. Horstmann, F. Single, A. Latz, *Curr. Opin. Electrochem.* **2019**, *13*, 61.
- [26] L. von Kolzenberg, A. Latz, B. Horstmann, *ChemSusChem* **2020**, *13*, 3901.
- [27] F. Buchner, K. Forster-Tonigold, B. Uhl, D. Alwast, N. Wagner, A. Groß, R. J. Behm, *ACS Nano* **2013**, *7*, 7773.
- [28] B. Uhl, M. Roos, R. J. Behm, T. Cremer, F. Maier, H. P. Steinrück, *Phys. Chem. Chem. Phys.* **2013**, *15*, 17295.
- [29] B. Uhl, F. Buchner, D. Alwast, N. Wagner, R. J. Behm, *Beilstein J. Nanotechnol.* **2013**, *4*, 903.
- [30] F. Buchner, B. Uhl, K. Forster-Tonigold, J. Bansmann, A. Groß, R. J. Behm, *J. Chem. Phys.* **2018**, *148*, 193821.
- [31] B. Uhl, F. Buchner, S. Gabler, M. Bozorgchenani, R. J. Behm, *Chem. Commun.* **2014**, *50*, 8601.
- [32] F. Buchner, M. Bozorgchenani, B. Uhl, H. Farkhondeh, J. Bansmann, R. J. Behm, *J. Phys. Chem. C* **2015**, *119*, 16649.
- [33] F. Buchner, K. Forster-Tonigold, M. Bozorgchenani, A. Gross, R. J. Behm, *J. Phys. Chem. Lett.* **2016**, *7*, 226.
- [34] F. Buchner, J. Kim, C. Adler, M. Bozorgchenani, J. Bansmann, R. J. Behm, *J. Phys. Chem. Lett.* **2017**, *8*, 5804.
- [35] F. Buchner, K. Forster-Tonigold, J. Kim, C. Adler, J. Bansmann, A. Groß, R. J. Behm, *J. Phys. Chem. C* **2018**, *122*, 18968.
- [36] K. Forster-Tonigold, F. Buchner, J. Bansmann, R. J. Behm, A. Groß, *Batteries Supercaps* **2022**, *5*, e202200307.
- [37] B. Uhl, M. Hekmatfar, F. Buchner, R. J. Behm, *Phys. Chem. Chem. Phys.* **2016**, *18*, 6618.
- [38] F. Buchner, K. Forster-Tonigold, J. Kim, J. Bansmann, A. Groß, R. J. Behm, *Chem. Mater.* **2019**, *31*, 5537.
- [39] K. Forster-Tonigold, J. Kim, J. Bansmann, A. Groß, F. Buchner, *ChemPhysChem* **2021**, *22*, 441.
- [40] F. Buchner, K. Forster-Tonigold, T. Bolter, A. Rampf, J. Klein, A. Groß, R. J. Behm, *J. Vac. Sci. Technol. A* **2022**, *40*, 023204.
- [41] I. Weber, J. Kim, F. Buchner, J. Schnaidt, R. J. Behm, *ChemSusChem* **2020**, *13*, 2589.
- [42] M. Nadhernä, J. Reiter, J. Moskon, R. Dominko, *J. Power Sources* **2011**, *196*, 7700.
- [43] N. Sánchez-Ramírez, B. D. Assresahegn, D. Bélanger, R. M. Torresi, *J. Chem. Eng. Data* **2017**, *62*, 3437.
- [44] R. Foulston, S. Gangopadhyay, C. Chiutu, P. Moriarty, R. G. Jones, *Phys. Chem. Chem. Phys.* **2012**, *14*, 6054.
- [45] F. Buchner, S. Fuchs, R. J. Behm, *J. Electroanal. Chem.* **2021**, *896*, 115497.
- [46] J. F. Moulder, W. F. Stickle, P. E. Sobol, K. D. Bomben, in *Handbook of X-Ray Photoelectron Spectroscopy* (Ed: J. Chastain), Perkin Elmer Corp., Eden Prairie **1992**.
- [47] A. B. Biedron, E. L. Garfunkel, E. W. Castner, S. Rangan, *J. Chem. Phys.* **2017**, *146*, 054704.
- [48] A. Jablonski, K. Wandelt, *Surf. Interface Anal.* **1991**, *17*, 611.
- [49] Y. Ge, T. Weidner, H. Ahn, J. E. Whitten, M. Zharnikov, *J. Phys. Chem. C* **2009**, *113*, 4575.
- [50] B. V. Merinov, S. V. Zybin, S. Naserifar, S. Morozov, J. Oppenheim, W. A. I. Goddard, J. Lee, J. H. Lee, H. E. Han, Y. C. Choi, S. H. Kim, *J. Phys. Chem. Lett.* **2019**, *10*, 4577.
- [51] H. Yildirim, J. B. Haskins, C. W. Bauschlicher, J. W. Lawson, *J. Phys. Chem. C* **2017**, *121*, 28214.
- [52] J. B. Haskins, H. Yildirim, C. W. Bauschlicher, J. W. Lawson, *J. Phys. Chem. C* **2017**, *121*, 28235.
- [53] E. Zintl, A. Harder, B. Dauth, *Z. Elektrochem.* **1934**, *40*, 588.
- [54] J. A. Lely, J. M. Bijvoet, *Recl. Trav. Chim. Pays-Bas* **1942**, *61*, 244.
- [55] H. Ott, *Z. Krist.* **1926**, *63*, 222.
- [56] A. Rabenau, H. Schulz, *J. Less Common Met.* **1976**, *50*, 155.
- [57] J. M. Kahk, G. S. Michelitsch, R. J. Maurer, K. Reuter, J. Lischner, *J. Phys. Chem. Lett.* **2021**, *12*, 9353.
- [58] C. J. Powell, A. Jablonski, in *NIST Electron Inelastic-Mean-Free-Path Database*, 1.1 ed., National Institute of Standards and Technology, Gaithersburg **2000**.
- [59] S. Tanuma, C. J. Powell, D. R. Penn, *Surf. Interface Anal.* **1994**, *21*, 165.
- [60] G. Kresse, J. Furthmüller, *Phys. Rev. B* **1996**, *54*, 11169.
- [61] G. Kresse, J. Furthmüller, *Comp. Mater. Sci.* **1996**, *6*, 15.
- [62] B. Hammer, L. B. Hansen, J. K. Nørskov, *Phys. Rev. B* **1999**, *59*, 7413.
- [63] S. Grimme, J. Antony, S. Ehrlich, H. Krieg, *J. Chem. Phys.* **2010**, *132*, 154104.
- [64] P. E. Blöchl, *Phys. Rev. B* **1994**, *50*, 17953.
- [65] G. Kresse, D. Joubert, *Phys. Rev. B* **1999**, *59*, 1758.
- [66] L. Köhler, G. Kresse, *Phys. Rev. B* **2004**, *70*, 165405.

Manuscript received: February 28, 2025

Revised manuscript received: May 7, 2025

Version of record online: